

TOPICAL REVIEW

Interfacial engineering for organic and perovskite solar cells using molecular materials

To cite this article: Anastasia Soultati *et al* 2020 *J. Phys. D: Appl. Phys.* **53** 263001




View the [article online](#) for updates and enhancements.

You may also like

- [Physics of defects in metal halide perovskites](#)
Chunxiong Bao and Feng Gao
- [Operational stability of perovskite light emitting diodes](#)
Qi Dong, Lei Lei, Juliana Mendes et al.
- [Applications and functions of rare-earth ions in perovskite solar cells](#)
Limin Cang, , Zongyao Qian et al.

Topical Review

Interfacial engineering for organic and perovskite solar cells using molecular materials

Anastasia Soultati¹ , Apostolis Verykios¹, Konstantina-Kalliopi Armadorou^{1,2},
Marinos Tountas^{1,3}, Veroniki P Vidali¹, Kalliopi Ladomenou⁴ , Leonidas Palilis⁵,
Dimitris Davazoglou¹, Athanassios G Coutsolelos⁵, Panagiotis Argitis¹
and Maria Vasilopoulou¹ 

¹ Institute of Nanoscience and Nanotechnology, National Center for Scientific Research 'Demokritos',
Agia Paraskevi 15341, Attica, Greece

² Department of Chemistry, National and Kapodestrian University of Athens, Zografos 15771, Greece

³ Department of Electrical & Computer Engineering, Hellenic Mediterranean University, Estavromenos,
Heraklion GR-71410, Crete, Greece

⁴ Department of Chemistry, Laboratory of Bioinorganic Chemistry, University of Crete, Voutes Campus,
Heraklion 70013, Crete, Greece

⁵ Department of Physics, University of Patras, Patras 26504, Greece

E-mail: acoutsol@uoc.gr, p.argitis@inn.demokritos.gr and m.vasilopoulou@inn.demokritos.gr

Received 30 November 2019, revised 24 February 2020

Accepted for publication 12 March 2020

Published 30 April 2020



Abstract

Organic and perovskite solar cells have recently emerged as promising candidates for next-generation solar energy technologies due to their low-cost solution-based fabrication over large areas even on flexible substrates, while offering the possibility of on-chip integration and patterning for custom-designed applications. A key concern over these emerging technologies is their poor operational stability. In a typical device architecture, the organic or perovskite absorber is usually inserted between an electron and a hole transport (extraction) layer in order to match the energetic differences present at the heterointerfaces with the respective contacts. As these layers considerably influence the device performance and operational stability, they have witnessed intense research efforts in recent years resulting in the development of novel materials. Conductive or insulating polymers, non-polymer molecular materials and transition metal oxides are among the most studied classes of interfacial materials. In this review article, we focus on the application of molecular materials, but excluding polymers, either organic or inorganic, to engineer the interfaces in these devices due to their ease of synthesis and facile functionalization of their structure to meet the requirements for successful device modification. We also include ionic compounds of well-defined stoichiometry such as CuSCN, ionic liquids and compounds of molecular anions as the polyoxometalates. We provide a comprehensive account of various molecular interlayers for organic and perovskite solar cell devices. We highlight the origin of enhanced performance and device lifetime and provide a detailed outlook for a focused future development of these materials.

Keywords: organic solar cells, perovskite solar cells, molecular materials, interface engineering

(Some figures may appear in colour only in the online journal)

1. Introduction

Organic (OSC) and perovskite (PeSC) solar cells are multilayer structures that consist of a photoactive layer embedded between two opposite contacts: an anode and a cathode electrode. In OSCs the photoactive material is based on a blend of a polymer donor (D) with an organic acceptor (A), whereas in PeSCs it consists of an organo-metal halide perovskite material of the general formula ABX_3 , where A is either an organic cation such as methyl ammonium (MA) or formamidinium (FA) or an inorganic cation (Cs, Rb), B is a six-valence metal (Pb, Sn) and X is halogen (Cl, Br, I). They have recently attracted much attention due to their significant advantages such as low cost, mechanical flexibility, light weight, and compatibility with flexible substrates. Through the design and synthesis of small-energy-gap polymer donors and with the advent of non-fullerene acceptors (NFAs), OSCs have steadily improved their power conversion efficiency (PCE) values to over 16% in single junctions and over 17.3% in tandem structures [1, 10]. In the case of PeSCs, certified efficiencies have recently surpassed 25% mainly due to their high molar absorptivity in a wide wavelength region, high electron and hole mobility and long charge carrier diffusion length of the order of a few millimeters [11, 18]. Besides the utilization of multifunctional photoactive materials and sophisticated device structures, the interface engineering of such devices using appropriate hole and electron transport interlayers plays a crucial role in the further improvement of device efficiency and, importantly, of operational stability [19, 20]. To enable sufficient device performance improvement, the properties of these interlayers should meet certain requirements such as: (1) well-aligned energy levels with those of the photoactive materials to allow for effective charge transport through the photoactive layer/photoactive absorber heterointerface, (2) a work function matched with that of the respective contact in order to increase the device built-in field and hence fasten the extraction of photogenerated carriers, (3) high charge carrier mobility, (4) high transparency, especially upon application in the device front contact when the light enters the device, (5) adequate photo and thermal stability, (6) good film-forming properties and (7) ease of deposition using low-cost methods. Recently, several types of interfacial materials have been explored for successful application in these devices. The most studied classes include inorganic transition metal oxides [21, 30], conjugated and insulating polymers [31, 34] and non-polymeric molecular materials [35, 36]. The basic characteristic of the latter class is that it uses assemblies of individual molecules as basic building blocks to reproduce conventional structures. These materials have properties that depend on their well-defined structure, the degree of order in the way the molecules are aligned and their crystalline nature. Small, delicate changes in molecular structure can totally alter the properties of the material in bulk and this represents one of their most intriguing characteristics for application as interfacial layers in OSCs and PeSCs. These changes can be obtained through soft routes, traditionally from organic, coordination, and supramolecular chemistry, and this opens unprecedented possibilities to the design of molecules with the desired size, shape, charge polarity, and

electronic properties, in response to the changing demands of solar cell technology. Among these demands is that molecular interfacial materials should exhibit tunable highest occupied molecular (HOMO) and lowest unoccupied molecular (LUMO) orbitals, charge carrier mobilities, and low-cost preparation and deposition methods. In this review we summarize recent developments on molecular materials used to engineer hole and electron transport interfaces. We highlight design guidelines and synthetic routes, implemented strategies and approaches for modifying the selective device interfaces with a large variety of molecular materials that are summarized as follows: small molecules, oligomers, molecular dyes such as porphyrins and phthalocyanines, ionic liquids, and inorganic molecular materials.

2. Working principles of organic and perovskite solar cells

2.1. Organic solar cells

Typically, OSCs use the bulk heterojunction (BHJ) design where a blend of a polymer donor and an organic acceptor forms separate phases that percolate throughout the device [37, 40]. As a universal design strategy, OSCs are commonly based on a trilayer architecture (figure 1), where the light-harvesting organic layer is inserted between two electrodes while appropriate charge (hole and electron) transport interlayers are also employed to improve charge extraction rates [20]. Upon photon absorption, a hole–electron pair (i.e. Frenkel exciton) is formed which then diffuses until it reaches a donor–acceptor heterointerface and splits to free carriers. The migration of those carriers, i.e. holes in the donor and electrons in the acceptor phases, towards and collection at the respective contacts creates the device photocurrent. The structure of the OSC could be either regular (forward) or inverted [41, 43]. In the regular architecture the device is built on the bottom transparent anode electrode (usually indium tin oxide, ITO). In inverted OSCs, the polarity is reversed and high-work-function (W_F) metals (such as Au, Al and Ag) are used for the fabrication of the top anode electrode, whereas the substrate, either ITO or fluorinated tin oxide (FTO), consists of the transparent cathode contact. Inverted OSCs are generally considered as more stable. One reason is that they do not require the use of a low- W_F metal as the top cathode electrode as the regular ones do. However, the selection of appropriate interfacial layers further improves the device stability.

2.2. Perovskite solar cells

PeSCs are a relatively new solar cell technology that has recently received much attention due to the rapid increase in its achieved efficiencies in less than a decade. The perovskite structure is comprised of a cubic cell with an ABX_3 unit per unit cell, where A at the corner of the unit cell and B at the center are organic and inorganic ions, respectively, and X is a halogen ion at the face-centered positions (figure 2(a)) [44, 45]. The perovskite structure can be in a Pm3m space group cubic symmetry, 12-fold and 6-fold coordination for

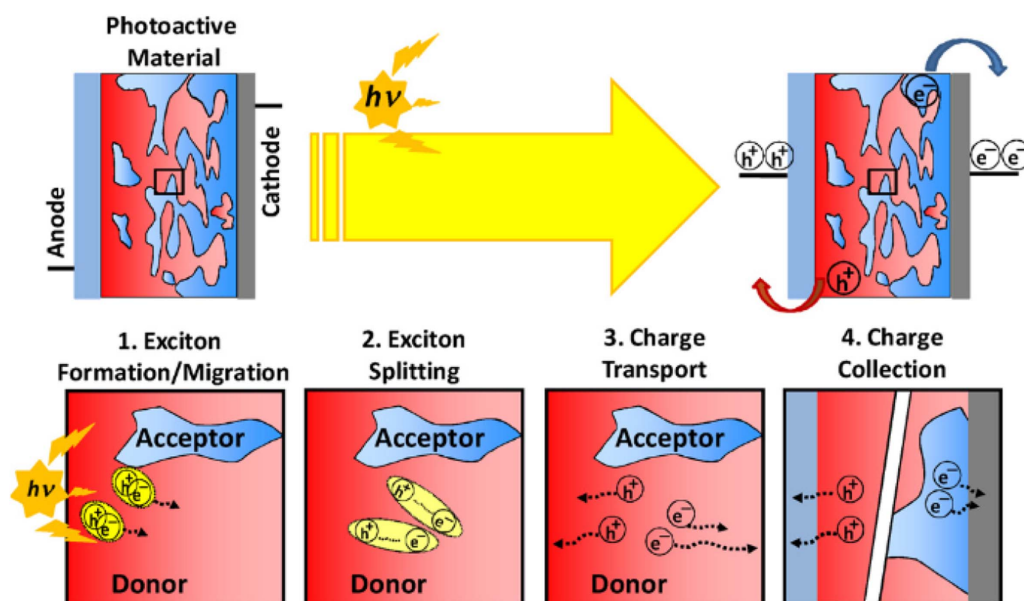


Figure 1. (Top) Schematic illustration of an OSC cell showing energy production upon illumination. (Bottom) Four key processes converting solar energy (photons) into electrical energy (charge flow). Reprinted from [20]. Copyright (2013), with permission from Elsevier.

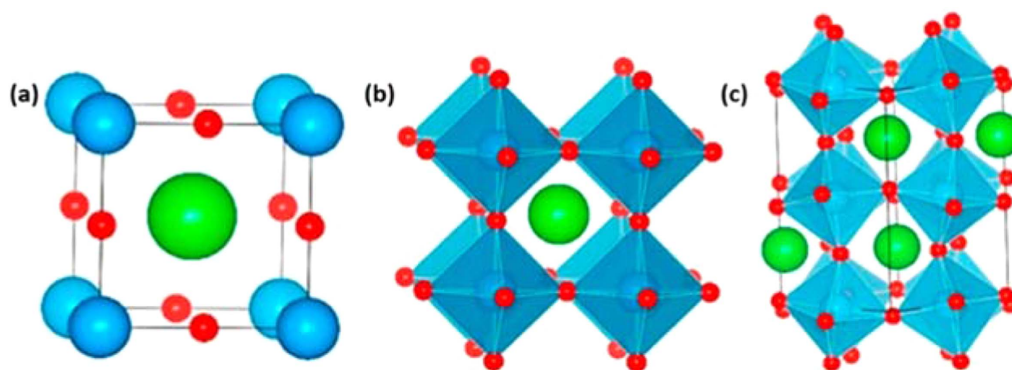


Figure 2. ABX₃ halide perovskite structure: (a) perovskite cubic unit cell, (b) BX₆ octahedral geometry, (c) tilted octahedral. Reproduced from [46]. CC BY 4.0.

A and B cations respectively, along with a BX₆ octahedral structure (figures 2(b), (c)). As perovskite materials with cubic symmetries have been reported to have the most desirable electric properties, a factor that seems to affect the symmetry of the cubic structure is the A cation dimensions, causing B–X bond distortion issues and undesirable octahedral tilting [46]. MAPbI₃ is the most widely studied perovskite composition as it was regarded as the most stable one, even though it requires high temperatures for successful crystallization, unlike MAPbCl₃ and MAPbBr₃ structures which crystallize even at room temperature. Perovskites usually form polycrystalline films that illustrate high charge carrier mobility, high carrier diffusion lengths, tunable bandgap and high absorption coefficients that lead to excellent photovoltaic behavior [47, 50]. The absorption of photons with energies above their bandgap values results in the formation of nearly free carriers that are transported through the conductive perovskite matrix and collected at the respective electrodes to form the device photocurrent.

3. Hole transport materials

Generally, both OSCs and PeSCs include five individual layers in their device structure: the hole selective contact, the hole transport/extraction layer (HTL/HEL), the organic or perovskite absorber, the electron transport/extraction layer (ETL/EEL) and the electron selective contact, as illustrated in figure 3. The HTL serves as the medium that enables efficient extraction of photogenerated holes from the absorber. In addition it should effectively block the extraction of opposite carriers (i.e. electrons) towards the hole selective contact. Higher efficiency can be therefore achieved owing to the role of an HTL in allowing fast hole transport and extraction towards the anode, to improve the selectivity of the anode interface, to suppress carrier recombination and block electron transfer towards the anode. In the regular OSC and inverted PeSC architectures it is inserted beneath the photoactive absorber, hence dictating the nanomorphology of the overlayer [51, 55]. It can be also an effective buffer medium to protect the organic

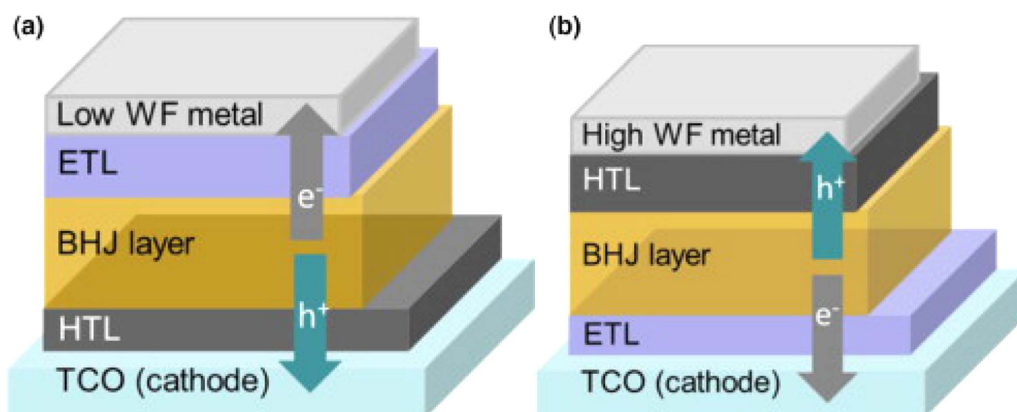


Figure 3. Schematic diagram for the regular (a) and inverted (b) OSC device structure. The electron transport layer (ETL) and hole transport layer (HTL) are adopted to form ohmic contact and extract charges at the cathode and anode, respectively. The arrows indicate the directions of electron and hole transport. Reprinted from [4], Copyright (2013), with permission from Elsevier.

or perovskite absorber from electrode-induced degradation. Therefore, it plays a key role in enhancing the device efficiency and stability in both the regular and inverted architectures [56, 60].

There are two major categories of molecular materials, other than polymers, serving as HTLs in OSCs and PeSCs: organic and inorganic compounds [61, 67]. The organic ones possess the advantage of requiring relatively low-temperature preparation routes compared to the inorganic counterparts [68, 71], which in certain cases require high-temperature sintering after deposition [72, 75]. Furthermore, the efficiency of OSCs and PeSCs using organic molecular HTLs is the highest to date among HTLs, but inorganic molecular HTLs allow high stability in OSCs and PeSCs and therefore represent a rapidly developing field [76, 92].

3.1. Inorganic molecular hole transport materials

3.1.1. Polyoxometalates. As polyoxometalates (POMs) have large electron affinities and a strong oxidation capability, their implementation as HTLs or effective p-type dopants for organic or perovskite photoactive and interfacial materials has also been explored in the last few years. Since the initial use of a commercially available Mo POM ($\text{PMo}_{12}\text{O}_{40}^{3-}$) cluster as an HTL in PTB7:PC₇₁BM-based OSCs [82], a universally enhanced PCE and cell stability have been demonstrated in various other OSC and PeSC architectures with different POMs, regardless of the employed organic [82, 89] or perovskite [90, 92] photoactive materials. Our group first implemented Keggin-type $\text{H}_3\text{PW}_{12}\text{O}_{40}$ and $\text{H}_3\text{PMo}_{12}\text{O}_{40}$ POMs and their Dawson counterparts ($(\text{NH}_4)_6\text{P}_2\text{W}_{18}\text{O}_{62}$ and $(\text{NH}_4)_6\text{P}_2\text{Mo}_{18}\text{O}_{62}$) as effective HTLs in OSCs [83]. Their high W_F of 6.0–6.2 eV and the position of their LUMO in combination with the presence of gap states just below the LUMO were found to be critical for efficient hole extraction. POMs with a deep LUMO level lying below the HOMO of the donor polymer in the photoactive blend combination led to interfacial p-doping of the polymer layer. Demonstration of solution-based, p-type doped, polymer semiconductor films by post immersion into a $\text{H}_3\text{PMo}_{12}\text{O}_{40}$ nitromethane solution

was also made by Aizawa *et al* [84], and Kolesov *et al* [85]. $\text{H}_3\text{PMo}_{12}\text{O}_{40}$ -doped films exhibited increased hole conductivity (5.5 S cm^{-1}) and a higher W_F (5.2 eV for PCDTBT) combined with an improved ambient photo-oxidative stability. As a result, OSCs based on various polymer donors such as P3HT and PCDTBT interfacially doped with POMs exhibited improved cell performance. Fuentes-Hernandez *et al* used acetonitrile as an alternative solvent for efficient, stable, P3HT p-type doping with $\text{H}_3\text{PMo}_{12}\text{O}_{40}$ that was extended to its bulk [86]. POM dopant molecules, facilitated by the solvent, were found to intercalate and reside in between the lamella of P3HT, physically enabling p-type doping to occur without distorting P3HT π - π stacking. Jia *et al* [87], and Guoqi *et al* [88], later explored annealing-free phosphomolybdic acid hydrate ($\text{H}_3\text{PMo}_{12}\text{O}_{40}$) as an anode buffer layer and in a nanocomposite with PEDOT:PSS, respectively, to improve the PCE of inverted PCDTBT- and P3HT:PC₇₁BM-based OSCs up to 6.57%. The enhanced efficiencies were ascribed to the fine energy-level matching and the facile surface modification of the organic layer (i.e. decreased contact angle and enhanced wettability) upon POM coating. Our group also proposed POMs as novel interconnecting layers in combination with n-type metal oxides in tandem OSCs, reaching an efficiency of 9.9% for an all solution-processed inverted structure [83]. Lu *et al* employed $\text{H}_3\text{PMo}_{12}\text{O}_{40}$ as the HTL of the interconnecting layer combined with ZnO and PEDOT:PSS in tandem OSCs [89], with efficiencies reaching 10.34% that were attributed to the excellent charge extraction properties of the employed POM HTL and the efficient recombination occurring at the interconnecting layer.

PeSCs with POMs as efficient HTLs or p-type dopants for the archetype Spiro-OMeTAD HTL have also been demonstrated with enhanced performance [90, 92]. Figure 4 depicts the energy level diagram and the architecture of PeSCs employing a representative $\text{PMo}_{11}\text{VO}_{40}^{4-}$ POM (abbreviation PMo_{11}V) p-type dopant on a Spiro-OMeTAD HTL. In a notable example, facile and enhanced oxidation of a spiro-OMeTAD HTL with an efficient hybrid Mo POM-based metal organic framework $[\text{Cu}_2(\text{BTC})_{4/3}-(\text{H}_2\text{O})_2]_6[\text{H}_3\text{PMo}_{12}\text{O}_{40}]_2$ dopant has been recently demonstrated resulting in PeSCs with

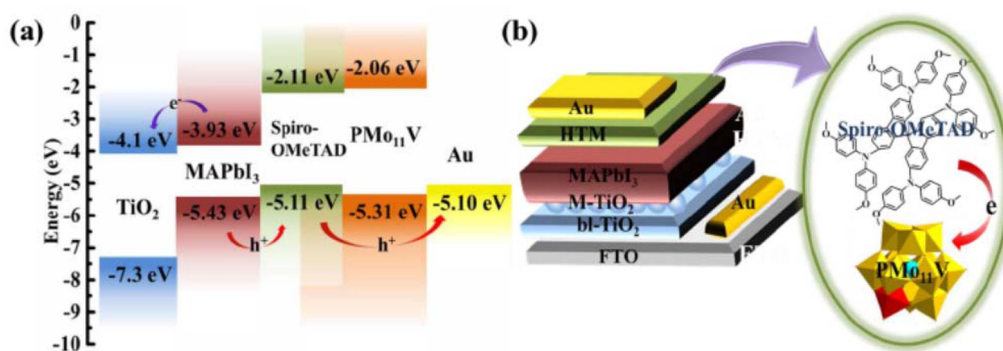


Figure 4. (a) Energy level diagram of the components of PeSCs employing a PMo₁₁V POM p-type dopant on a Spiro-OMeTAD HTL. (b) Schematic architecture of the fabricated PeSCs incorporating the POM-doped HTL. Reprinted with permission from [90]. Copyright (2017) American Chemical Society.

a superior fill factor (FF) of 0.80 and an enhanced PCE of 21.44% as well as improved long-term stability in ambient conditions [91].

3.1.2. CuSCN. More recently, another wide-bandgap p-type semiconductor, namely CuSCN, with a hole mobility of $\sim 0.5 \text{ cm}^2 \text{ Vs}^{-1}$ and a suitable W_F of $\sim 5.2 \text{ eV}$ to match the ionization energy I_E of most organic semiconductors and perovskites was proposed. A CuSCN HTL has been employed in different OSC (regular and inverted type) and PeSC configurations (n-i-p and p-i-n type) with PCEs reaching 8.07% for PBDTTPD:PC₆₁BM-based OSCs [76], and 17.50% for MAPbI₃- [77] and 20.40% for CsFAMAPbI_{3-x}Br_x-based PeSCs [78], respectively. CuSCN was also found to be beneficial in regulating the morphology (i.e. grain size) and enhancing the crystallinity and the perovskite surface coverage. In order to increase its hole conductivity, p-type molecular doping with strong organic electron acceptors such as C₆₀F₄₈ [79] and F₄-TCNQ [80] has been successfully demonstrated. The p-type doped CuSCN layers were employed as HTLs in OSCs and PeSCs. Improved PCEs of 6.60% for PCBTBT:PC₇₀BM-based OSCs [79] and 14.40% for p-i-n type/MAPbI₃-based PeSCs [80] have been reported accompanied by lower dark current, enhanced shunt and lower series resistance. Enhanced solar cell performance was attributed to the enhanced hole mobility and the facile hole transfer as a result of the Fermi level shift towards the valence band of the p-type doped CuSCN, thus reducing the interfacial energetic mismatch.

To synergistically exploit the advantageous effects of both CuI and CuSCN in enhancing solar cell performance, solution-processed CuI/CuSCN composite films were proposed as effective HTLs in p-i-n type MAPbI_{3-x}Cl_x-based planar PeSCs [81]. While CuI and CuSCN as HTLs resulted in PCEs of 14.53% and 16.66%, respectively, a significantly enhanced PCE of 18.76% was recorded for the PeSCs with the composite HTL. The improved performance of the composite compared to the pristine layers was attributed to the smoother perovskite film quality obtained upon introducing CuSCN as an underlayer for perovskite growth and its higher electrical conductivity.

3.2. Organic molecular hole transport materials

3.2.1. Small molecules. Small molecules have been extensively studied and used as anode interfacial layers in emerging photovoltaic technologies, including organic and perovskite solar cells. Interestingly, the application of small molecules as surface modifiers affects the W_F of the underlying anode, resulting in favorable energy level alignment at the HTL/photoactive layer interface. In addition, modification of the nanomorphology of the active layer (both organic and perovskite absorber film) coated on top of them, in regular OSC and inverted PeSC architectures, respectively, has proven beneficial to device performance. The insertion of small-molecule HTLs in inverted OSCs has also contributed to device stability, protecting the underlying photoactive layer from moisture and oxygen penetration. Several types of small molecules bearing amine groups have been successfully applied as HTLs in OSCs. This is because amine groups form large interfacial dipoles causing significant vacuum-level shift at the respective contact. Representative examples are those based on (N,N'-diphenyl-N,N'-bis(3-methylphenyl)-(1,1'-biphenyl)-4,4'-diamine)-cores. Lu *et al* designed a series of such materials with different carboxyl side chains, in particular acetic acid, butyric acid or hexanoic acid, and referred to them as TPDA, TPDB and TPDH, respectively [93]. These authors demonstrated that all these materials were soluble in polar solvents, whereas the quality of the film was dependent on the length of the molecule's side-chain. Owing to their adequate hole mobility and appropriate energetics, these materials enabled sufficient improvement in the device performance when applied as HTLs. In another study, Subbiah *et al* [94] investigated a different amine-group molecule that has been widely applied in the field of organic light-emitting diodes, namely 4,4',4''-tris[(3-methylphenyl)phenylamino]triphenylamine (MTDATA). They used this material as the hole transport interlayer along with MoO₃ in inverted OSCs based on a PDTS-BTD:PC₇₁BM blend. The incorporated MTDATA HTL facilitated vertical phase separation of the photoactive blend film, as well as the formation of band bending of the PDTS-BTD HOMO level, which was beneficial to the device performance. Acidic molecules present a different class of small molecular materials that have been

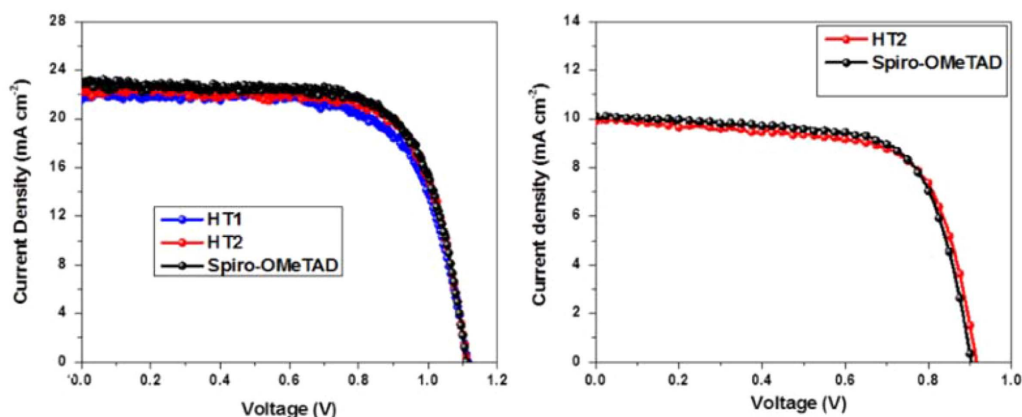


Figure 5. PeSC performance using Spiro-OMeTAD or H1, H2 as the HTLs. Reprinted from [109], Copyright (2016), with permission from Elsevier.

studied as HTLs in OSCs as they can also induce significant vacuum-level shifts. In a representative example, Choi *et al* [95] applied 4-chloro-benzoic acid (CBA) as a hole transport interlayer and surface modifier in PTB7:PC₇₁BM-based OSCs. The introduction of a CBA layer between the active layer and the ITO anode significantly modified the surface properties of ITO, hence changing its surface tension while also upwardly shifting the vacuum level and causing a higher value of W_F of the modified contact. An improvement in the device performance was also demonstrated, attributed to the enhanced light-harvesting and the efficient hole transport from the active layer towards the anode. Various small molecules have been also incorporated in PeSCs between the anode electrode and the perovskite absorber to improve the hole transport, and thus the device performance. The most popular small-molecule hole transport layer is spiro-OMeTAD (2,20,7,70-Tetrakis-(N,N-di-4-methoxyphenylamino)-9,9-spirobifluorene). It was first used by Bach *et al* in 1998 [96] as a solid hole conductor in dye-sensitized solar cells (DSSCs). However, as it shows low conductivity ($\sim 10^{-5}$ S cm⁻¹) in its pristine form, most relevant works in PeSCs usually enable appropriate materials to dope Spiro-OMeTAD. The most successful examples of such dopants include tris(2-(1H-pyrazol-1-yl)pyridine)cobalt(III) (FK102) [97] and (tris(2-(1H-pyrazol-1-yl)-4-tert-butylpyridine)cobalt(III) tri[bis(trifluoromethane) sulfonimide]) (FK209) [98] as well as Li-TFSI along with t-BP [99]. Li *et al* [100] followed a different path by using acids of moderate strength as additives in Spiro-OMeTAD, the most promising of which was AcOH demonstrating an improved device performance. Besides the application of dopants, several groups attempted the modification in the chemical structure of Spiro-OMeTAD to induce desirable optoelectronic properties. Jeon *et al*, given that the methoxy group was responsible for the oxidation potential of this material, studied the effect of changing its position and synthesized three different molecules, where the -OMe group was in the ortho, para or meta position termed as po-Spiro-OMeTAD, pp-Spiro-OMeTAD, and pm-Spiro-OMeTAD, respectively [101]. They obtained better device performance for po-Spiro-OMeTAD. In this context,

Burschka *et al* shifted the methoxy groups from the para to meta position, which increased the oxidation potential of the resultant molecule [102]. These authors also replaced the methyl chain in the -OMe group with larger alkyl chains and synthesized the compounds Spiro-m-OMe, Spiro-3,5-OMe, Spiro-p-tBu, Spiro-3,5-tBu, Spiro-3,5-mixed, Spiro-OMe-TPA and Spiro-p-OHex. They found that Spiro-OMe-TPA and Spiro-m-OMe exhibited certain advantages against degradation [103]. In the same context, Hu *et al* also modified the structure of Spiro-OMeTAD molecules by replacing methoxy groups with ethyl and thiomethyl groups and synthesized Spiro-E and Spiro-S respectively. The photophysical and hole transport properties of the modified molecules, along with their influence on the morphology of perovskite film coated on top of them, were investigated [104]. Several other attempts to modify the chemical structure of Spiro-OMeTAD led to successful results [105, 108]. One of the most successful approaches was the design and synthesis by Grätzel *et al* [105] of a novel material with a 4,4'-spiro[cyclopenta[2,1-*b*:3,4-*b'*]dithiophene] core and triarylamine terminal units (Spiro-CPDT), whereas another spiro[fluorene-9,90-xanthene]-based HTL (termed as X60) also proved beneficial [107]. However, due to the ease of oxidation of Spiro-OMeTAD several groups focused their works on the development of alternative small molecular materials for use as HTLs in PeSCs. Fluorene compounds represent one of the most successful classes of newly developed materials [109, 113]. For instance, Hua *et al* prepared fluorene-based molecules HT1 and HT2 [109] (figure 5). These molecules were highly soluble in common organic solvents and their synthesis was low cost, in contrast with the expensive synthesis of Spiro-OMeTAD. In addition, Saliba *et al* designed a dissymmetric fluorene-dithiophene molecule (FDT) as a low-cost alternative to Spiro-OMeTAD [110]. This small-molecule-based-PeSC was easily dissolved in toluene, which is relatively environmentally friendly. Due to its superior characteristics it yielded a record device conversion efficiency of over 20%.

However, donor-acceptor-donor (D-A-D) HTLs proved more resistant to moisture than Spiro-OMeTAD, leading to better long-term device stability. As an example, Sun

and colleagues [114] designed a Spiro-OMeTAD derivative, 2,6,14-tris(50-(N,N-bis(4-methoxyphenyl) aminophenol-4-yl)-3,4-ethylenedioxythiophen-2-yl)-tritycene (TET), the production cost of which was unexpectedly low. The application of a 30 nm film as an HTL exhibited good stability making it promising for commercialization of PeSCs. In the same direction, Jeon *et al.* developed the most promising Spiro-based molecule for use as an HTL in PeSCs, in particular (N2,N2', N7,N7'-tetrakis(9,9-dimethyl-9H-fluoren-2-yl)-N2,N2',N7,N7'-tetrakis(4-methoxyphenyl-9,9'-spirobi[fluorene]-2,2',7,7'-tetraamine) (DM) [115]. The device's high certified PCE of 22.60% was ascribed to the well-matched energy levels between the HTL and the perovskite absorber, leading to a significant enhancement of V_{oc} . DM-based devices also showed superior thermal stability by maintaining 95% of their initial performance after 500 h of thermal annealing.

Furthermore, in order to avoid the multistep and expensive synthesis of Spiro-MeOTAD, other small molecules have been synthesized and employed as HTLs in perovskite solar cells, such as thiophene, triphenylamine, triazatruxene, and carbazole derivatives. Small molecules based on thiophene cores with arylamine side groups present ease of synthesis [116, 118], making these molecules successful Spiro-OMeTAD alternatives in terms of both performance and overall characteristics. For instance, Zimmermann *et al.* [117] created small molecules based on an anthra[1,2-b:4,3-b':5,6-b'':8,7-b''']-tetrathiophene (ATT) core, namely ATT-OMe, ATT-OBu and ATT-OMe, where the methoxy groups on the triarylamine sites were replaced by butoxy and hexoxy groups showing improved solubility. The employed small molecules facilitated hole extraction whereas the perovskite PL signal was also quenched at the interface between the active layer and the HTL, proving the successful hole transfer [117]. In a similar strategy, García-Benito *et al.* [119] synthesized an isomeric benzotrithiophene (BTT)-cored material crosslinked with p-methoxytriphenylamines, called BTT-4 for application as an HTL in PeSC. The impressive rate of hole extraction was attributed to the cis arrangement of the sulfur atoms facing each other in its core.

Besides thiophenes, triphenylamine derivatives have been also used as HTLs in perovskite photovoltaics. They exhibit the advantages of higher moisture stability compared to Spiro-based compounds, while they do not require the use of dopants [120, 127]. As an example, a series of novel materials named Tetra-TPA, Tri-TPA, and Bi-TPA were designed and used as HTLs in PeSCs by Park and his team [123]. The conductivity of those materials was enhanced when more TPA groups were introduced in the molecular structure. Application of these novel molecules in PeSCs at the perovskite/anode interface increased PCE values and improved the device stability. A method to enhance the hole mobility of such materials was developed by Murata *et al.* [124], which designed, synthesized and characterized small molecules that belong to the series of partially oxygen-bridged triarylamine substituents connected to an azulene main body (termed as Azl-1). Azl-1-based PeSCs displayed an improved performance attributed to the

enhanced hole mobility and the improved hole-collection efficiency at the interface between the perovskite absorber and the HTL. Another family of alternatives to Spiro-OMeTAD small molecules is truxene derivatives [128, 129]. Park *et al.* [128] engineered novel molecules, synthesized by Suzuki coupling, for which the methoxy units, in function with their number, could control carrier extraction and recombination in PeSCs. The device with the trux-OMeTAD that contained three methoxy units showed the greatest efficiency since those units promoted passivation of the interface between the HTL and the active layer (figure 6).

Carbazole derivatives have also been successfully employed as hole transport materials in perovskite devices [130, 131]. In most cases, these carbazole compounds were attached to a small molecule core to improve its optoelectronic properties. Examples include methoxydiphenylamine-substituted carbazoles [132], materials with a core unit of methylenebenzene, linked with diphenylamine-substituted carbazole fragments [133], 2,2',7,7'-tetrakis(N,N'-di-p-methoxyphenylamine)-N,N'-bicarbazole molecules [134], carbazole-based material with OMeTAD groups outside of its core [135] and carbazole-based enamine molecules [136]. The use of these molecules in PeSCs yielded high efficiency values while the starting materials were inexpensive, thus creating cheaper alternatives for large-scale applications.

However, the catalogue of small molecular materials applied as HTLs in PeSCs is still large [137, 146]. It also includes donor-acceptor (D-A) or D-A-D compounds. For instance, Liu *et al.* [137], reported a D-A π -conjugated small molecule termed as DERDTS-TBDT. This molecule employed alkylthienyl-substituted benzo[1,2-b:4,5-b'] dithiophene (TBDT) as its core, dithienosilole (DTS) as an electron-donating part and 3-alkyl rodanine as an electron-withdrawing part. A high PCE was demonstrated for the DERDTS-TBDT HTL-based PeSC, attributed to high hole mobility and well-matched energy levels between the HTL and perovskite material (figure 7).

In addition, Zhu *et al.* designed the thiothene-quinoxaline-based molecule TQ2 with a D-A-D configuration as a low-cost alternative material to Spiro-OMeTAD [140]. The TQ2-based device showed higher conversion efficiency compared to Spiro-OMeTAD while also strengthening the device stability. Moreover, bipyridine-based molecules were also applied as HTLs in PeSCs [144] (figure 8). The electron-withdrawing ability of bipyridine molecules tuned the HOMO level of these molecules, facilitating hole extraction from the perovskite absorber towards the selective electrode. However, one critical issue was always the application of small-molecule HTLs via solution processing at low temperature. Small molecules such as TPASBP (4,4'-bis(4-(di-p-toyl)aminostyryl)biphenyl) and TPASB (1,4'-bis(4-(di-p-toyl)aminostyryl)benzene) were applied with a low-temperature solution-processed method (substrate temperature around 100 °C) on the p-i-n PeSCs [145]. These small molecules facilitated the growth of perovskite films when spin-coated on top of them, resulting in improved hole extraction at the HTL/perovskite layer interface. Table 1 summarizes the molecular structures and device performance for small-molecule HTLs discussed here.

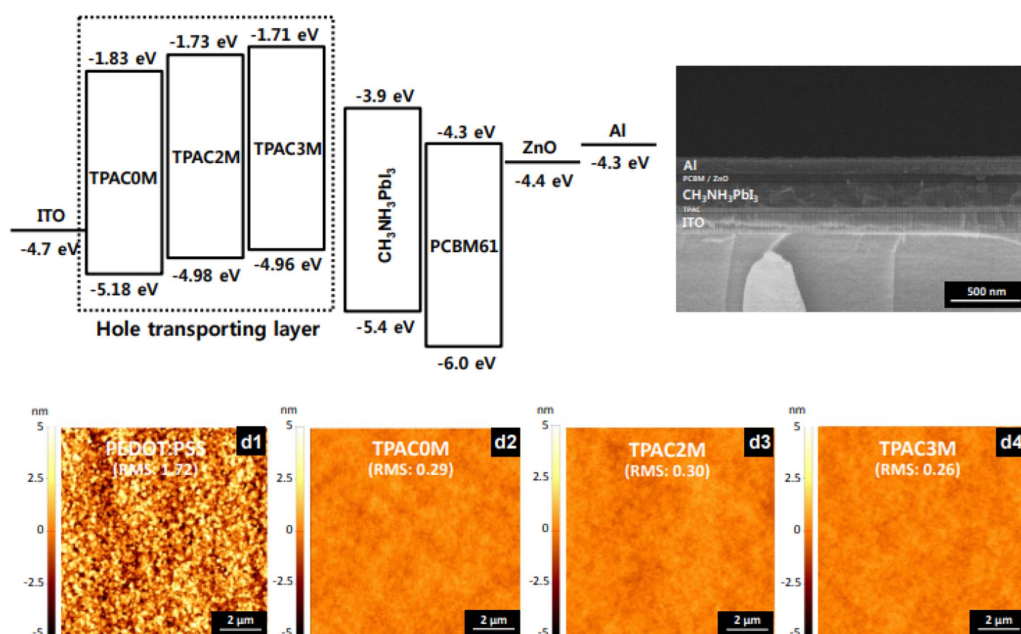


Figure 6. Energy level of each layer of PeSCs and cross-sectional SEM of TPAC-based perovskite solar cell (TPAC3M-based device as a representative) (up). AFM height images of (d1) PEDOT:PSS, (d2) TPAC0M, (d3) TPAC2M, and (d4) TPAC3M on ITO electrode. RMS values of PEDOT:PSS, TPAC0M, TPAC2M, and TPAC3M on ITO are 1.72, 0.29, 0.30, and 0.26 nm, respectively (down). Reproduced from [128] with permission of The Royal Society of Chemistry.

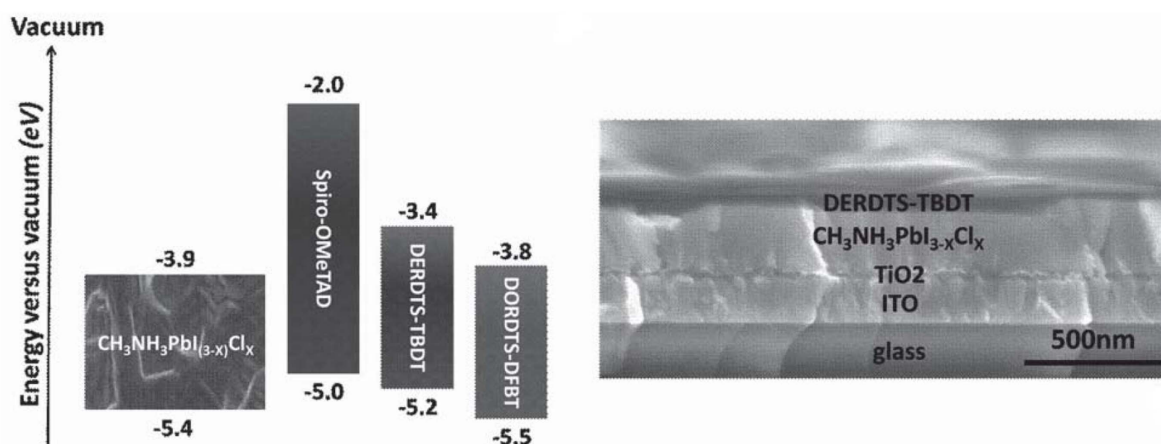


Figure 7. Energy level diagram of the lead halide perovskite, Spiro-OMeTAD, DERDTS-TBDT, and DORDTS-DFBT. SEM image of cross-sectional structure of the representative device without top electrode. [137] John Wiley & Sons. Copyright (2016) WILEY-VCH Verlag GmbH & Co. KGaA, Weinheim.

3.2.2. Porphyrins. Porphyrins are a promising class of organic molecules that can be used for the construction of high-performance organic and perovskite solar cells. Inspired by natural photosynthesis, porphyrins and their analogues have been extensively used in numerous artificial photosynthetic devices and the synthesis of photovoltaic materials [147, 151]. In dye-sensitized solar cells (DSSCs) a donor- π -acceptor zinc metallated porphyrin possesses the highest record in power conversion efficiency (13%) [152]. Porphyrins feature remarkable properties such as high molar absorption coefficients, electrical and optical properties that can be tuned by numerous structural modifications. These chromophores also demonstrate thermal and moisture stability, effective electron transfer [153] and low cost of production.

Porphyrins play an important role in the understanding and development of organic and perovskite solar cells. In OSCs porphyrins were widely used as dyes in the p-type donor phase combined with fullerene or perylene derivatives as the acceptor phase [154, 158]. However, Amirhossein *et al* [159] introduced their use as hole transport materials. In particular, these authors employed the composite poly(3,4-ethylenedioxythiophene) polystyrene sulfonate/iron (III) porphyrin supported on S and N co-doped graphene quantum dots (PEDOT:PSS/FeTSPP@S,N:GQDs) as HTL in OSCs. An enhancement in the device performance was observed along with the device stability, compared with the reference OSCs using simple PEDOT:PSS as HTL. This improvement was attributed to the benzoid-quinoid transition and the energy

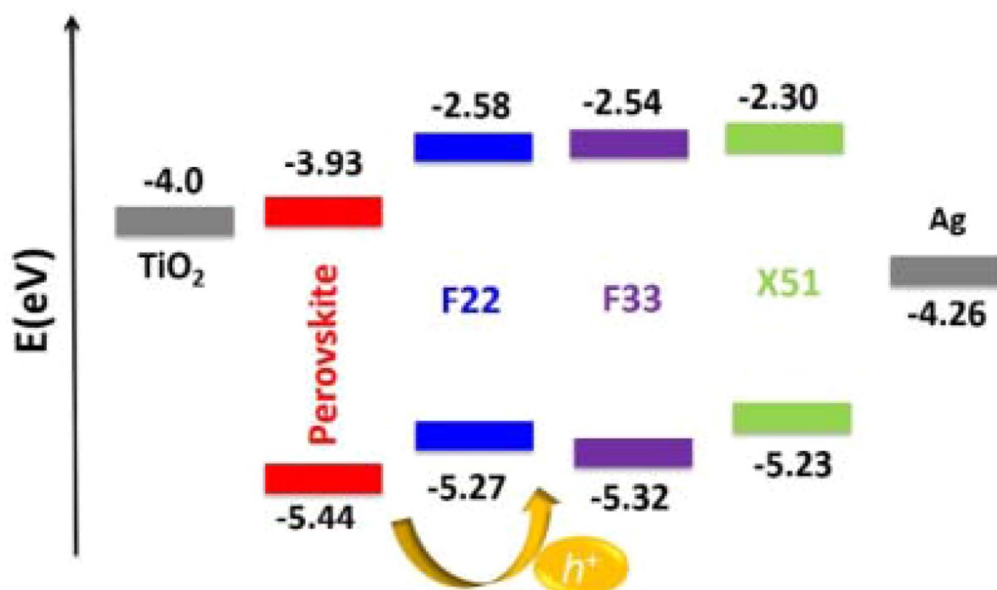


Figure 8. Energy diagram for the new HTMs F22 and F33. X51 is included for comparison. [144] John Wiley & Sons. Copyright (2017) WILEY-VCH Verlag GmbH & Co. KGaA, Weinheim.

level alignment at the PEOdT:PSS/FeTSPP@S, N:GQD interface leading to enhanced hole transport and improved conductivity. Similarly, the use of porphyrins as hole transport materials proved to be valuable in the enhancement of efficiency and stability of PeSCs [160,167]. In 2016 the first example of a porphyrin-based HTL in PeSCs was reported in the literature [160]. Two symmetrical porphyrins Y2 and Y2A2 were synthesized featuring meso 5,15-bis(ethynylaniline) structure and in the two opposite positions bearing alkoxyphenyl groups. These molecules included butyl (Y2) and dodecyl chains (Y2A2) in order to ensure solubility and to improve the morphology of the film. The HOMO levels of compounds Y2 and Y2A2 were -5.25 eV and -5.10 eV, respectively, which were very close to that of Spiro-OMeTAD (-5.22 eV). PeSCs were prepared by spin-coating porphyrin compounds on the perovskite/TiO₂ layer. The PCE values of the porphyrin-based devices were inferior compared to that of Spiro-OMeTAD but the device with Y2 exhibited much improved stability. Sequentially, Chiang *et al* modified the chemical structures of these compounds and prepared the dimeric porphyrin conjugates WT3 and YR3 based on Y2 [161]. The HOMO levels of YR3 and WY3 were -5.11 eV and -5.14 eV, respectively. They were hence located above the valence band minimum (VBM) of the perovskite, meaning that they could create the appropriate driving force for hole extraction from the perovskite layer. Moreover, the LUMOs of both dimers were quite high in order to avoid possible electron current leakage. However, besides modification of the initially applied compounds, several groups were then introduced to the application of alternative porphyrin molecules such as the symmetric porphyrins ZnP and CuP [162]. These porphyrins could be easily synthesized with direct pyrrole condensation with the appropriate benzaldehyde. The HOMO energy level of CuP was measured at -5.37 eV and of ZnP at -5.29 eV. These were both higher than that

of perovskite (-5.56 eV). The LUMO levels of both were higher than that of perovskite, minimizing the charge recombination. The main advantage of these materials was their greater stability compared to Spiro-OMeTAD. Therefore, Jung *et al* [163] subsequently modified their structure in order to study the effect of structural differences in the device. All studied porphyrin devices showed improved air stability and slightly lower PCEs compared to the Spiro-OMeTAD device. The same group introduced fluorine atoms at the phenyl ring linked to the porphyrin [164]. The fluorinated devices PZn-2FTPA and PZn-3FTPA showed increased charge injection/transfer and better hole transport mobility compared to the non-fluorinated porphyrin PZn-TPA. In another effort to obtain high PCEs and further stability of PSCs, porphyrins with alternative metal cores were selected such as the two porphyrins Co(II)P and Co(III)P [165]. Specifically, these porphyrins were of type ABAB containing methoxy-substituted oxyalkyl chains in order to induce solubility, and methoxy substituted triphenyl amine groups in order to promote efficient charge transport. The Co(II)/Co(III) couple had already been reported in dye-sensitized solar cells [166]. Moreover, inspired by nature, sinapoyl malate was used at the interface of TiO₂ and the perovskite in order to improve the UV stability and the contact between the two phases. Sinapoyl malate is the natural sunscreen of plants and it was applied to protect the perovskite film from the UV radiation. Figure 9 presents the chemical structures of the most popular examples of porphyrin molecules used as HTLs in PeSCs.

4. Electron transport materials

The electron transport layer (ETL), which serves as the medium that injects the photogenerated electrons from the

Table 1. Summary of the chemical structures of small molecules used as HTLs in PeSCs, the device structure and the performance characteristics.

HTM	V _{oc} (V)	J _{sc} (mA cm ⁻²)	FF (%)	PCE (%)	Active layer	Dopant	Ref
Spiro-OMeTAD	0.878	9.100	29.00	2.30	(FAPbI ₃) _{1-x} (MAPbBr ₃) _x	none	[104]
Spiro-OMeTAD	0.940	9.600	62.00	5.60	(FAPbI ₃) _{1-x} (MAPbBr ₃) _x	FK102	[105]
Spiro-OMeTAD	1.140	23.600	73.00	20.10	(FAPbI ₃) _{1-x} (MAPbBr ₃) _x	FK209	[106]
Spiro-OMeTAD	0.997	20.570	70.00	14.32	MAPbI ₃	Li-TFSI, t-BP	[107]
Spiro-OMeTAD	0.925	19.040	73.00	12.93	MAPbI ₃	F4-TCNQ	[107]
Spiro-OMeTAD	1.080	22.100	75.00	17.80	FA _{0.85} CS _{0.15} PbI ₃	AcOH	[108]
pp-Spiro-OMeTAD	1.000	20.100	71.10	14.90	MAPbI ₃	Li-TFSI, t-BP	[109]
pm-Spiro-OMeTAD	1.010	21.100	65.20	13.90	MAPbI ₃	Li-TFSI, t-BP	[109]
po-Spiro-OMeTAD	1.020	21.200	77.60	16.70	MAPbI ₃	Li-TFSI, t-BP	[109]
Spiro-E	1.070	18.240	80.00	15.75	MAPbI ₃	none	[111]
Spiro-S	1.060	19.150	78.00	15.92	MAPbI ₃	none	[111]
Spiro-CPDT	0.970	19.300	72.00	13.40	MAPbI ₃	none	[112]
X59	1.130	23.400	73.00	19.80	(FAPbI ₃) _{0.85} (MAPbBr ₃) _{0.15}	Li-TFSI, t-BP, FK209	[113]
X60	1.140	24.400	71.00	19.80	(FAPbI ₃) _{0.85} (MAPbBr ₃) _{0.15}	Li-TFSI, t-BP, FK209	[114]
H11	1.120	23.300	72.00	19.80	(FAPbI ₃) _{0.85} (MAPbBr ₃) _{0.15}	Li-TFSI, t-BP, FK209	[115]
H12	1.070	22.700	69.00	16.60	(FAPbI ₃) _{0.85} (MAPbBr ₃) _{0.15}	Li-TFSI, t-BP, FK209	[115]
HT1	1.120	22.000	70.00	17.20	(FAPbI ₃) _{0.85} (MAPbBr ₃) _{0.15}	Li-TFSI, t-BP, FK209	[116]
HT2	1.110	22.300	73.00	18.00	(FAPbI ₃) _{0.85} (MAPbBr ₃) _{0.15}	Li-TFSI, t-BP, FK209	[116]
FDT	1.150	22.700	76.00	20.10	(FAPbI ₃) _{0.85} (MAPbBr ₃) _{0.15}	Li-TFSI, t-BP, FK209	[117]
X54	0.950	21.300	67.00	13.60	(FAPbI ₃) _{0.85} (MAPbBr ₃) _{0.15}	Li-TFSI, t-BP, FK209	[118]
X55	1.150	23.400	77.00	20.80	(FAPbI ₃) _{0.85} (MAPbBr ₃) _{0.15}	Li-TFSI, t-BP, FK209	[118]
DDOF	1.101	22.370	79.00	19.40	(FAPbI ₃) _{0.85} (MAPbBr ₃) _{0.15}	Li-TFSI, t-BP, FK102	[119]
Yih-2	1.020	22.180	71.00	16.06	MAPbI ₃	LiTFSI, t-BP	[120]
TET	1.070	21.960	81.40	19.10	MAPbI ₃	Li-TFSI	[121]
DM	1.110	24.800	81.00	22.30	(FAPbI ₃) _{0.85} (MAPbBr ₃) _{0.15}	LiTFSI, t-BP	[122]
H111	1.080	19.800	72.00	15.40	MAPbI ₃	LiTFSI, t-BP	[123]
H112	1.070	20.000	71.00	15.20	MAPbI ₃	LiTFSI, t-BP	[123]
ATT-OMe	1.070	21.800	78.10	18.10	(FAPbI ₃) _{0.85} (MAPbBr ₃) _{0.15}	Li-TFSI, t-BP, FK209	[124]
ATT-OBu	1.050	20.900	78.30	17.30	(FAPbI ₃) _{0.85} (MAPbBr ₃) _{0.15}	Li-TFSI, t-BP, FK209	[124]
ATT-Ohex	1.030	19.600	77.80	15.70	(FAPbI ₃) _{0.85} (MAPbBr ₃) _{0.15}	Li-TFSI, t-BP, FK209	[124]
Z26	1.132	23.590	75.00	20.10	MAPbI ₃	Li-TFSI	[125]
BTT-4	1.090	23.040	75.30	18.97	(FAPbI ₃) _{0.85} (MAPbBr ₃) _{0.15}	Li-TFSI	[126]
ST1	1.060	21.100	66.00	15.40	MAPbI ₃	none	[127]
Z33	1.090	20.500	66.00	15.40	MAPbI ₃	none	[128]
Z34	1.060	21.200	70.00	16.10	MAPbI ₃	none	[128]
Z1011	1.090	20.500	70.00	16.30	MAPbI ₃	none	[129]
Tetra-TPA	1.050	22.000	78.00	18.00	MAPbI ₃	Li-TFSI, t-BP	[130]
Tri-TPA	1.030	21.400	74.40	16.40	MAPbI ₃	Li-TFSI, t-BP	[130]
Di-TPA	1.030	20.500	73.30	15.50	MAPbI ₃	Li-TFSI, t-BP	[130]
Azl-1	1.040	20.700	73.00	15.70	MAPbI ₃	LiTFSI, t-BP, FK209	[131]
PCP-TPA	1.040	22.000	78.00	17.80	MAPbI ₃	LiTFSI, t-BP	[132]
YN2	1.110	23.150	75.00	19.27	(FAPbI ₃) _{0.85} (MAPbBr ₃) _{0.15}	Li-TFSI	[133]
Si-OMeTPA	1.070	23.080	77.17	19.06	MAPbI ₃	F4-TCNQ	[134]
Trux-OMeTAD	1.020	23.220	79.00	18.60	MAPbI ₃	none	[135]
KR131	1.146	20.700	75.00	17.70	(FAPbI ₃) _{0.85} (MAPbBr ₃) _{0.15}	none	[136]
KR133	1.133	20.400	68.00	15.80	(FAPbI ₃) _{0.85} (MAPbBr ₃) _{0.15}	none	[136]
SGT-405	1.020	20.300	71.30	14.80	MAPbI ₃	Li-TFSI, t-BP, FK209	[137]
SGT-411	1.000	18.600	67.20	13.00	MAPbI ₃	Li-TFSI, t-BP, FK209	[138]
V886	1.090	21.400	73.40	16.90	MAPbI ₃	Li-TFSI, t-BP, FK209	[139]
V911	1.103	22.400	76.30	18.72	(FAPbI ₃) _{0.85} (MAPbBr ₃) _{0.15}	none	[140]
2,7 BCz-OMeTAD	1.089	22.380	72.50	17.60	MAPbI ₃	none	[141]
CzPAF-SBF	1.090	20.910	73.92	16.85	MAPbI ₃	Li-TFSI	[142]
V950	1.070	22.500	74.00	17.80	(FAPbI ₃) _{0.85} (MAPbBr ₃) _{0.15}	none	[143]
DERDTS-TBDT	1.050	21.200	71.80	16.20	MAPbI _{3-x} Cl _x	none	[144]
BF002	1.01	21.560	65.00	14.20	MAPbI ₃	Li-TFSI, t-BP, FK102	[145]
BF003	1.03	21.220	64.00	14.07	MAPbI ₃	Li-TFSI, t-BP, FK102	[145]

Table 1. Continued.

HTM	V_{oc} (V)	J_{sc} (mA cm ⁻²)	FF (%)	PCE (%)	Active layer	Dopant	Ref
TAPC	1.040	22.320	81.15	18.80	MAPbI ₃	none	[146]
TQ2	1.120	22.550	77.67	19.62	MAPbI ₃	Li-TFSI	[147]
JY5	1.060	21.060	76.00	16.87	MAPbI _{3-x} Cl _x	LiTFSI, t-BP	[148]
JY6	1.066	21.390	81.00	18.54	MAPbI _{3-x} Cl _x	LiTFSI, t-BP	[149]
TPA-ANT-TPA	1.030	21.070	79.60	17.50	MAPbI ₃	none	[150]
F22	1.050	21.260	79.00	17.71	MAPbI _{3-x} Cl _x	none	[151]
F33	1.110	21.010	79.00	18.48	MAPbI _{3-x} Cl _x	none	[151]
TPASBP	1.040	20.700	80.00	17.40	MAPbI ₃	none	[152]
TPASB	1.050	20.800	80.00	17.60	MAPbI ₃	none	[152]
DNA-CTMA	1.040	20.850	73.15	15.86	MAPbI ₃	none	[153]

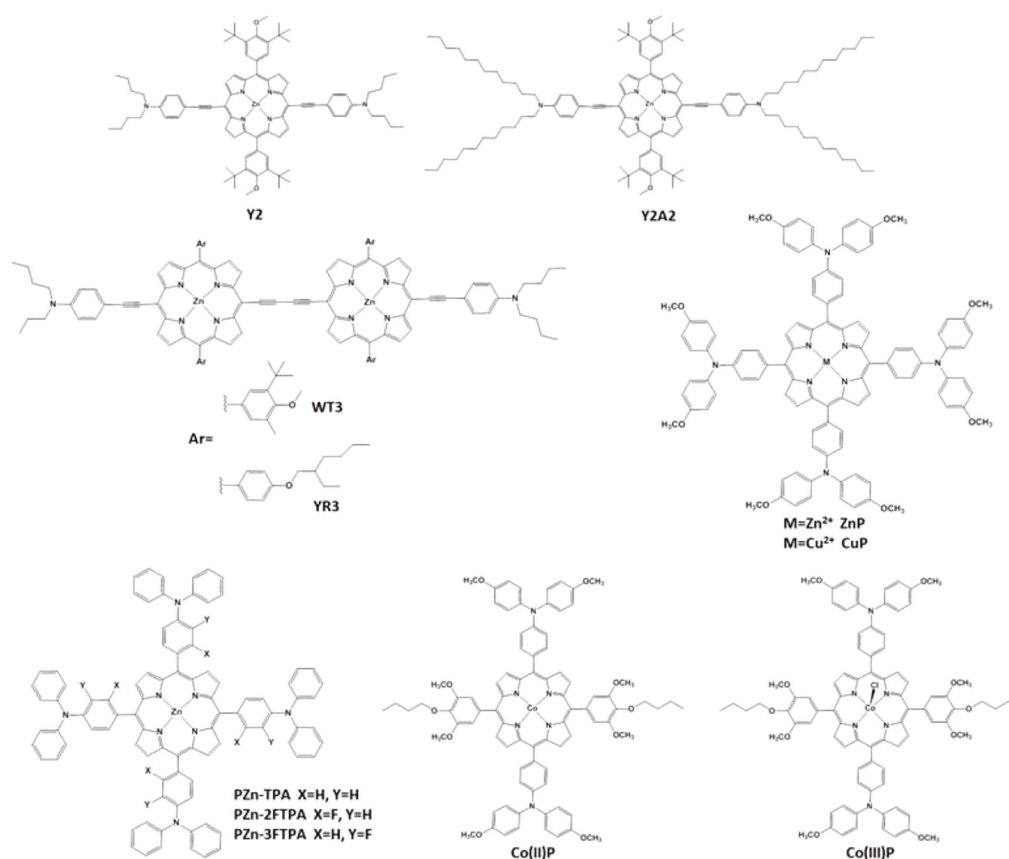


Figure 9. Chemical structure of porphyrins used as HTLs in PeSCs.

absorber to the electron-selective contact, is also vital for efficient OSCs and PeSCs [168, 178]. In general, efforts devoted to the development of efficient ETLs are relatively few. This is associated with the fact that inorganic metal oxides such as zinc oxide (ZnO), titanium dioxide (TiO₂) and tin dioxide (SnO₂) provide both high efficiency and good stability when used as ETLs in both types of device. However, with the exploration of a variety of novel organic and perovskite semiconductor materials there is increasing need to design novel, high-performing ETLs that will accomplish perfect matching (i.e. energetic) with the novel absorbers to maximize the device performance [179, 190]. Moreover, the ETLs should possess appropriate physical properties, robustness and completely cover the organic/perovskite layer to prevent

moisture and air ingress, which degrades the stability of these devices [191, 195].

4.1. Organic molecular electron transport materials

4.1.1. Fullerene derivatives. Fullerene derivatives have for many years been the go-to materials for the active layer of OSCs. They are the n-type acceptor materials that together with a p-type polymer donor create the BHJ blend. With the recent rapid advances in perovskites, they are now broadly used as ETLs in PeSCs and especially in inverted planar structures, where the ETL is deposited on top of the perovskite layer. Sun *et al* [196] showed that a fullerene ETL is a strong electron acceptor, which forms anion- π interactions

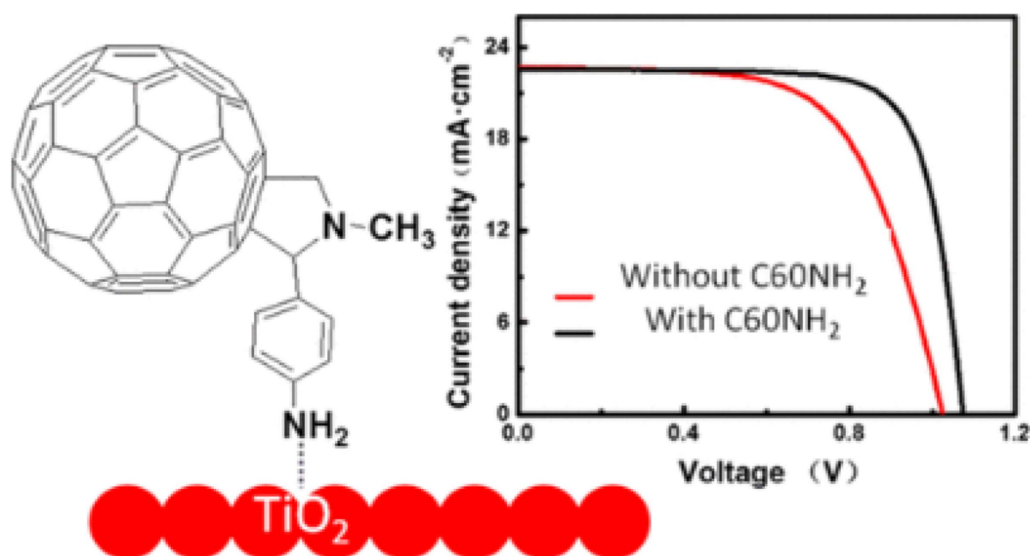


Figure 10. PeSC performance using amino-functionalized fullerenes as electron transport interlayers. Reprinted with permission from [203]. Copyright (2019) American Chemical Society.

enhancing the performance and the stability of PeSCs. Shao *et al* [197] demonstrated PCBM's ability to restrain the hysteresis of PeSCs via trap-state passivation, and later showed that solvent annealing makes PCBM more ordered, which leads to enhancements in V_{oc} and PCE [198]. Luo *et al* [199] have also fabricated an inverted PeSC structure with PCBM as the ETL and reached an improved PCE of 20.9%. Chiang and Wu [200] used PCBM to fabricate a two-step bulk heterojunction PeSC consisting of a perovskite–PCBM layer that showed a smooth morphology, increased V_{oc} and FF with no hysteresis (figure 10). In regular PeSCs, one of the most commonly used ETLs is TiO_2 . A viable strategy to overcome the low conductivity of TiO_2 is to add a thin layer of PCBM between the ETL and the perovskite [201]. Cao *et al* [202] used a hydroxylated fullerene, fullerenol, as an interlayer that led to enhanced PCE, and Chen *et al* [203] used a $C_{60}NH_2$ fullerene derivative as a passivation interlayer that helped to reduce hysteresis and improve device performance and stability. Pyridine-functionalized fullerene derivatives that completely replaced the TiO_2 layer have also been synthesized and used in devices, which showcased enhanced PCE and significantly suppressed hysteresis while working as a passivation layer for the perovskite absorber [204, 205]. An ETL that is also widely applied in PeSCs is SnO_2 , but the defects of its surface and the hysteresis it introduces to the devices limits its applications. Fullerene derivatives have been recently used to modify the SnO_2 ETL, by suppressing charge recombination via passivation of defects, improving photovoltaic performance with negligible hysteresis and enhancing device stability [206, 207].

A widely studied strategy to overcome the limitations of PCBM is the doping of fullerene derivatives by adding a small amount of other materials into the PCBM solution. Yan *et al* [208] used conductive fullerene surfactants such as FPPI, Bis-FPPI, Bis-FIMG, and Bis-FITG as ETLs in both organic and perovskite solar cells, which enhanced electron

transfer and photovoltaic performance, while being insensitive to the thickness of the interlayer. Reduced graphene oxide (rGO) is also widely used as a dopant of PCBM. Kakavelakis *et al* [209] doped PCBM with 5% rGO, which enhanced the electron-transport ability of PCBM, and the PCE was improved from 12.9% to 14.5%. Chang *et al* [210] used cetyl trimethyl ammonium bromide (CTAB) surfactant as a PCBM dopant which appeared to enhance its electron transport properties and improved electrical conductivity fivefold. The results indicated that the doping takes place via anion-induced transfer of electrons between PCBM and bromide anions. The devices delivered a high PCE not only in PeSCs but also in large-area solar cells.

A series of hydrophilic fullerene derivatives were designed by Xing *et al* [211], by combining fullerenes with electron-rich functional groups, where they incorporated them as alternative ETLs in place of PCBM (figure 11). They found that oligoether (OE) side groups could passivate the trap states of the perovskite as well as reduce the W_F of the cathode electrode, which led to enhanced photovoltaic properties and reduced hysteresis. This was attributed to the reduced barrier between the ETL and cathode as well as to better electron transport. Instead of hydrophilic, hydrophobic functional groups were also tested by Bai *et al* [212], which were attached onto fullerenes to make a more water-resistant layer. They also doped the fullerene layer with methylammonium iodide, which resulted in an increase in conductivity by more than 100-fold. PCE and FF were enhanced and the hydrophobic layer improved moisture and water stability of PeSCs by retaining 90% of their efficiency after 30 d of ambient air exposure. Enhanced air stability was also achieved by Zhu *et al* [213], who developed a novel fullerene derivative F- C_{60} that was combined with the bis- C_{60} surfactant to form a robust interlayer. This approach led to improved device stability in ambient air, due to its hydrophobic characteristics, as well as improvement of PCE.

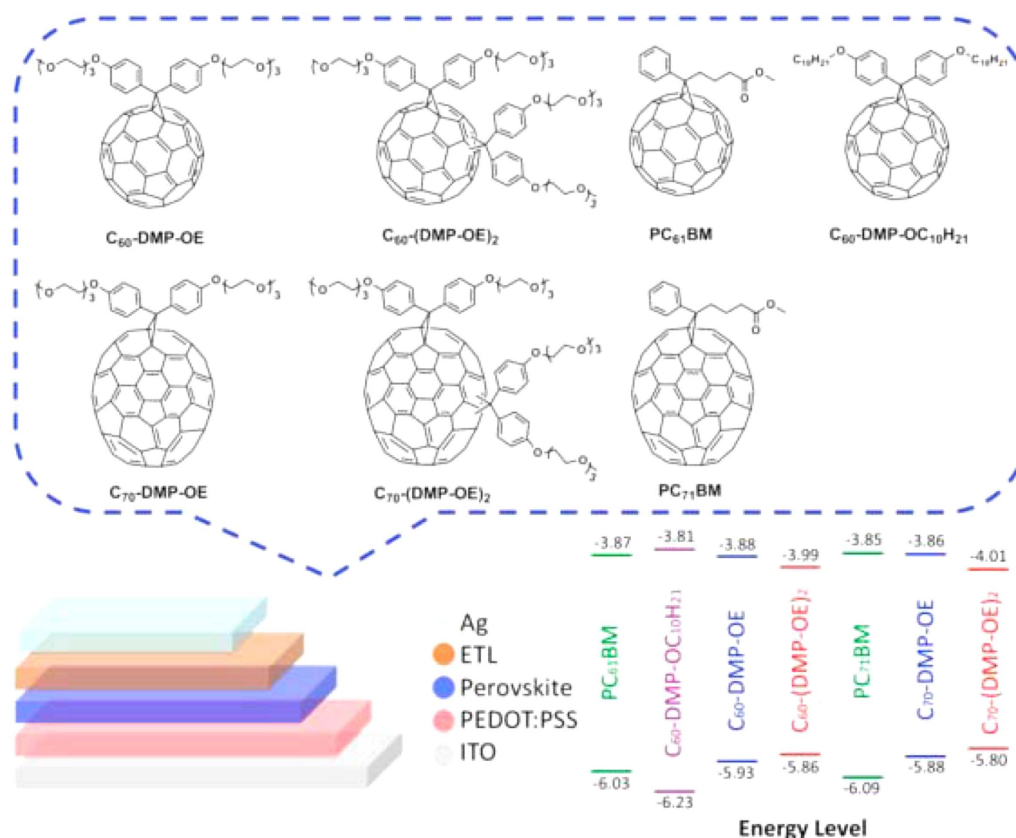


Figure 11. Device architecture of PeSCs, chemical structures and energy levels of C₆₀-DMP-OE, C₆₀-(DMP-OE)₂, C₆₀-DMP-OC₁₀H₂₁, C₇₀-DMP-OE, C₇₀-(DMP-OE)₂, PC₆₁BM and PC₇₁BM fullerene derivatives. Reprinted from [211], Copyright (2016), with permission from Elsevier.

Wide-bandgap PeSCs are used in tandem devices to help surpass the Shockley–Queisser limit and achieve higher PCEs than those of single-junction devices. Khadka *et al* [214] used a long-alkyl-chain-substituted fullerene derivative (C₆₀MC₁₂) to tune the ETL of a wide-bandgap mixed-halide PeSC. They demonstrated an enhanced PCE and a record V_{oc} of 1.24 V by reducing the recombination losses via passivating the interface recombination centers, due to the high crystallinity of the fullerene derivatives.

In OSCs there are also several studies on the application of fullerene derivatives as buffer layers and as ETLs in both regular and inverted structures. Jung *et al* [215] managed to enhance the performance and the stability of OSCs, by using a self-assembled PEG-C₆₀ buffer layer that also helped with oxidative stability. A bis-adduct C₆₀ surfactant was used by O'Malley *et al* [216] to modify the alignment of the energy levels between the active layer and the cathode, independently of the metal used as the cathode. The active layer consisted of a low-bandgap polymer and PC₇₁BM. They witnessed an increase in V_{oc} , which led to an enhancement of PCE and stability. Similar results were found by Page *et al* [217], who incorporated C₆₀-N and C₆₀-SB as cathode-independent buffer layers. Enhanced PCE was obtained, regardless of cathode selection, which ranged between Al, Ag, Cu, and Au. Li *et al* [218], synthesized two PCBM derivatives, PCBDAN and PCBDANI, which were used as cathode buffer layers

to replace Ca. They showed identical or slightly enhanced photovoltaic performance, but they were able to significantly improve the device stability through replacing the unstable Ca cathode.

Fullerene derivatives as interfacial layers in OSCs have also been studied in inverted structures. An alcohol-soluble fullerene derivative, namely B-PCPO, was developed by Duan *et al* [219], and was used as an interlayer between ITO and the active layer (figure 12). This improved electron transport and collection and it also decreased the W_F of ITO. The enhancement in V_{oc} and slight increase in FF led to a significant increase in the OSC device performance. Other fullerene derivatives that have been synthesized and used in inverted OSCs as ETLs between the cathode and the active layer include Bis-OMe FPI [220], C₆₀-ETA [221], DMAPA-C₆₀ [222] and C₆₀-PEGA [223]. The use of those in inverted OSCs gave an enhanced PCE in all cases, compared to the widely used ETL ZnO.

Instead of replacing the ZnO ETL layer, Liao *et al* [224] doped it with a hydroxyl-containing derivative, which led to a ZnO-C₆₀ cathode. This induced electron collection enhancement and also produced a cathode surface, rich of fullerene derivative that promoted electron conductivity and led to a high enhancement of PCE. Similarly, Liu *et al* modified ZnO with an ether-chain-functionalized fullerene derivative (C₆₀-2EPM). The ZnO/C₆₀-2EPM interface helped

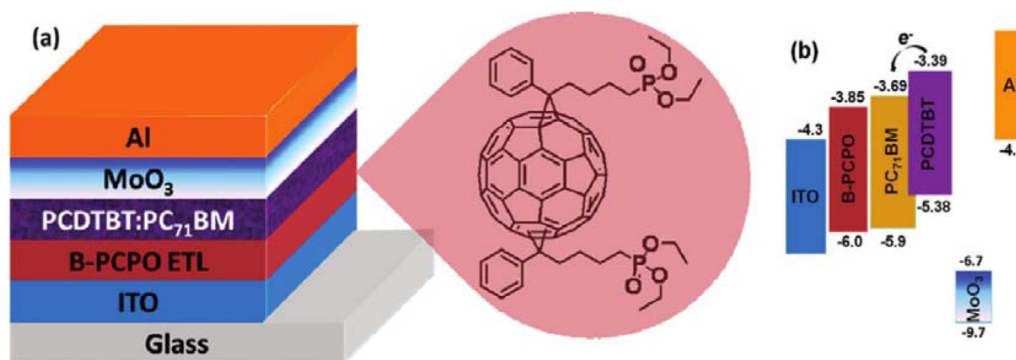


Figure 12. (a) Inverted OSC with B-PCPO as ETL and (b) energy level diagram of the materials used in device fabrication. Reproduced from [219] with permission of The Royal Society of Chemistry.

with electron transfer, increased photocurrent and enhanced PCE [225].

Recently Guo *et al* [226], studied the use of PCBM as an interlayer between the active layer and the ETL. It led to improvement in J_{sc} , FF, and PCE by inducing phase separation of the BHJ that enhanced exciton dissociation and charge transfer. The modified morphology of the surface also helped, by increasing light absorption.

4.1.2. Porphyrins. Porphyrins have also been used as efficient ETLs in both high-performance OSCs and PeSCs. The ability of porphyrins to self-assemble and to form organized structures was successfully applied in OSCs by Vasilopoulou *et al* [227]. One metal-free and one metallated porphyrin were inserted between the organic photoactive layer based on P3HT:PC₆₁BM and the metal cathode in OSCs. Significant efficient improvement was obtained when the metal-free porphyrin was added. The efficiency increased to 4.4% relative to 2.7% for the reference device without the porphyrin layer. It was reported that the metal-free porphyrin adopted a face-to-face molecular orientation parallel to the substrate, while the metallated one self-assembled with edge-to-edge molecular orientation. Therefore, the type of organization of the material affected the photovoltaic performance of the system. In another report, the same metal-free porphyrin with indene-C₆₀ bis-adduct (ICBA) increased the PCE of the BHJ organic photovoltaic cell to 7.13% [228]. Furthermore, a water-soluble porphyrin FNEZnP-OE was synthesized bearing two amino-functionalized fluorenes linked to the porphyrin core with ethylene linkages and two polar 3,4-bis-[2-(2-methoxy-ethoxy)-ethoxy]-phenyls [229]. This porphyrin was used as a cathode interfacial material in OSCs based on either PTB7/PC₇₁BM or PTB7-Th/PC₇₁BM blends. The devices with FNEZnP-OE as the electron transport layers achieved PCEs of 8.52% and 9.16%, respectively. This high performance was due to the porphyrin π -conjugated system achieved by the ethynylene linkages and they are very promising cathode interfacial materials.

There is another example of a porphyrin molecule that was specially designed in order to act as a cathode interfacial modifier in OSCs [230]. The porphyrin compound TPPtriazinegly₂Zn possessed two carboxylic acids

as anchoring groups onto TiO₂ and a triazine electron-withdrawing spacer. This porphyrin was deposited on TiO₂ in PTB7:PC₇₁BM-based OSCs. A PCE of 8.37% was obtained, which was improved by 34% compared to the control device with a PCE of 6.52%.

Despite the extensive use of porphyrins as HTLs in PeSCs, there is only one example of their use as electron transport materials in perovskite solar cells [231]. This example involves the triazine-substituted Zn porphyrin bearing two anchoring groups for efficient attachment onto TiO₂. It was inserted between the TiO₂ layer and the CH₃NH₃PbI₃ perovskite film to serve as the ETL [231]. The porphyrin-based device exhibited a PCE of 16.87% which was 12% higher compared to the reference cell (15.01%). The modified device also retained 86% of the initial PCE after 200 h, while the reference cell degraded to 67% due to faster decomposition of CH₃NH₃PbI₃ to PbI₂, indicating that porphyrin was not only an efficient ETL but also protected the perovskite layer from penetration of moisture and oxygen molecules. Figure 13 presents the chemical structures of porphyrin molecules used as ETLs in OSCs and PeSCs.

4.1.3. Non-fullerene oligomers. The most commonly used electron transport materials in organic and perovskite solar cells are fullerene-based materials and their derivatives, such as [6,6]-phenyl-C₆₁-butyric acid methyl ester (PCBM), as already mentioned. The devices with fullerene derivatives as ETLs have achieved high performance due to high electron mobility, three-dimensional transport and surface passivation of the photoactive layer. However, they suffer from some obstacles, such as poor ambient and thermal stability, monotonous energy level tunability and high cost. In the past few years, intense research efforts have been devoted to the development of alternative, non-fullerene materials to be used as ETLs in order to overcome these obstacles. Fei Huang's group [232] developed an amino-functionalized polymer (PFN-2TNDI) as an alternative material to replace the commonly used PCBM in p-i-n planar PeSCs. A reduced W_F of the metal cathode due to formation of a large interfacial dipole caused by the assembly of amines and the surface passivation of the perovskite film increased the charge transport to these non-fullerene based devices, which showed a PCE of 16.17%

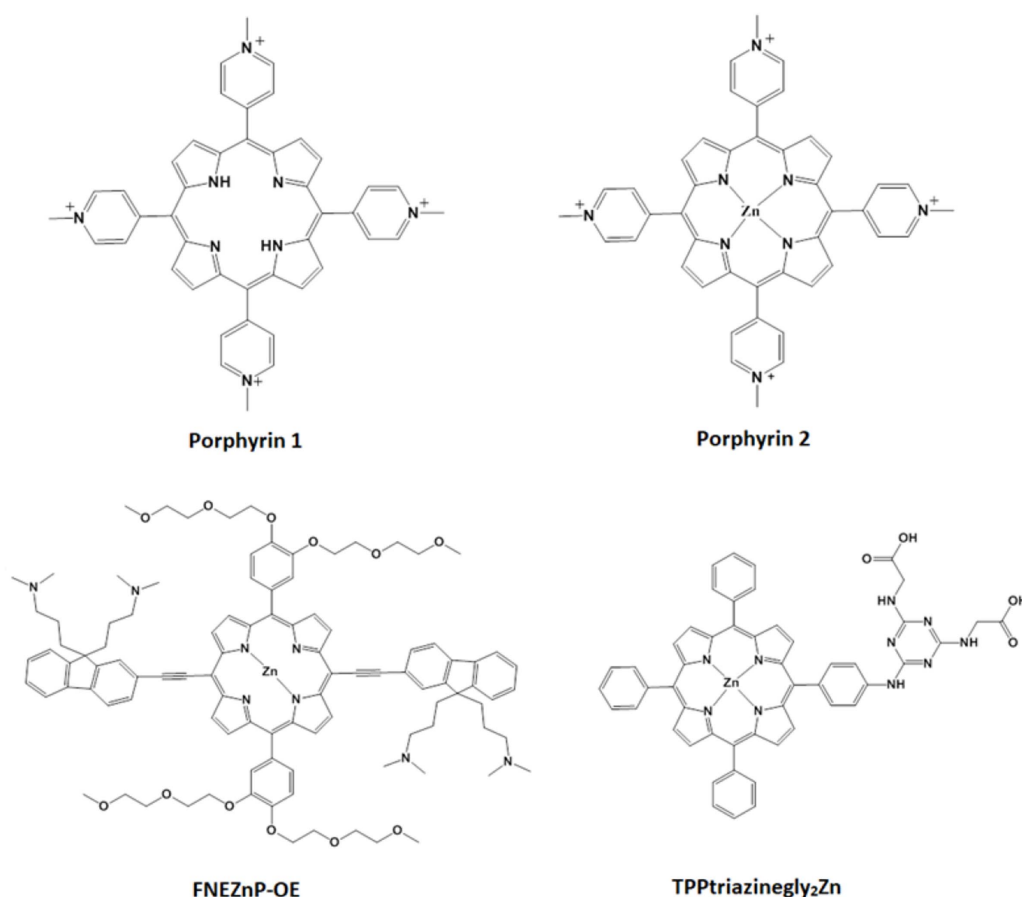


Figure 13. Chemical structure of porphyrins used as ETLs in OSCs and PeSCs.

against 12.7% of the fullerene-based ones. A series of perylene diimide (PDI)-based polymers (Px-PDIs) with different conjugated units, such as vinylene (V), thiophene (T), selenophene (Se), dibenzosilole (DBS) and cyclopentadithiophene (CPDT), were also introduced as alternative electron transport materials in p-i-n PeSCs [233]. They exhibited some attractive characteristics such as tunable energy levels, controllable aggregate formation, and smooth film formation. Sang Hyuk Im's group [234] used a non-fullerene compound, N,N'-bis(phenylmethyl)naphthalene-1,4,5,8-tetracarboxylic diimide (NDI-PM), as an ETL in two different planar perovskite solar cells, based on $\text{CH}_3\text{NH}_3\text{PbI}_3$ (MAPbI₃) and $\text{HC}(\text{NH}_2)_2\text{PbI}_{3-x}\text{Br}_x$ (FAPbI_{3-x}Br_x). The MAPbI₃- and FAPbI_{3-x}Br_x-based devices with the non-fullerene ETL achieved PCE values of 18.4% and 19.6%, respectively, which were competitive with the reference devices (18.9% and 20%). Furthermore, the Hirshfeld surface analysis and void structure characterization showed that the devices based on non-fullerene compounds exhibited better thermal stability because of the stronger hydrogen bonds. In another study, perylene derivative TPE-PDI₄ was applied in inverted perovskite solar cells as an ETL and interfacial layer between the photoactive layer and the C₆₀ [235]. The modified devices achieved high PCE values of 16.29% and 18.78% when TPE-PDI₄ was used as an ETL and interlayer, respectively. Moreover, the better water resistibility of the perylene

derivative than that of the PCBM enhanced the ambient stability after 200 h.

Yaus *et al* [236] designed and synthesized two tryxene-bridged trimers, TR-PDI₃ and Tr-PDI₃-C. The TR-PDI₃-based device achieved a PCE of 17.45% along with reduced hysteresis. When the same compound was used as an interlayer incorporated between the C₆₀ and the perovskite absorber a high PCE of 19.83% was achieved. Furthermore, two NDI derivatives 4-(5-((4,5-bis(octylthio)-1,3-dithiol-2-ylidene)methyl)thiophen-2-yl)-2,7 dioctylbenzo[lmn][3,8]phenanthroline-1,3,6,8(2H,7H)-tetraone (DS1) and 4,9-bis(5-((4,5-bis(octylthio)-1,3-dithiol-2-ylidene)methyl)thiophen-2-yl)-2,7 dioctylbenzo[lmn][3,8]phenanthroline-1,3,6,8(2H,7H)-tetraone (DS2) were designed and synthesized by Qichun Zhang's group [237] in order to replace the PCBM ETL in PeSCs. These two derivatives bearing various donor and acceptor units facilitated the charge transport via S-I or S-Pb interactions, while the presence of dithiol units decreased the energy bandgap. The DS1- and DS2-based devices achieved a PCE of 9.6% and 11.4%, respectively.

Following a different strategy, Yang's group [238] synthesized two π -conjugated molecules, rigid ladder-type derivatives of the ITCPTC with two side chains thiophene (ITCPTC-Th) and selenophene for use as ETLs in PeSCs. Specifically, the ITCPTC-Th device exhibited a PCE of 17.11%. The smaller surface roughness and more ordered molecular packing

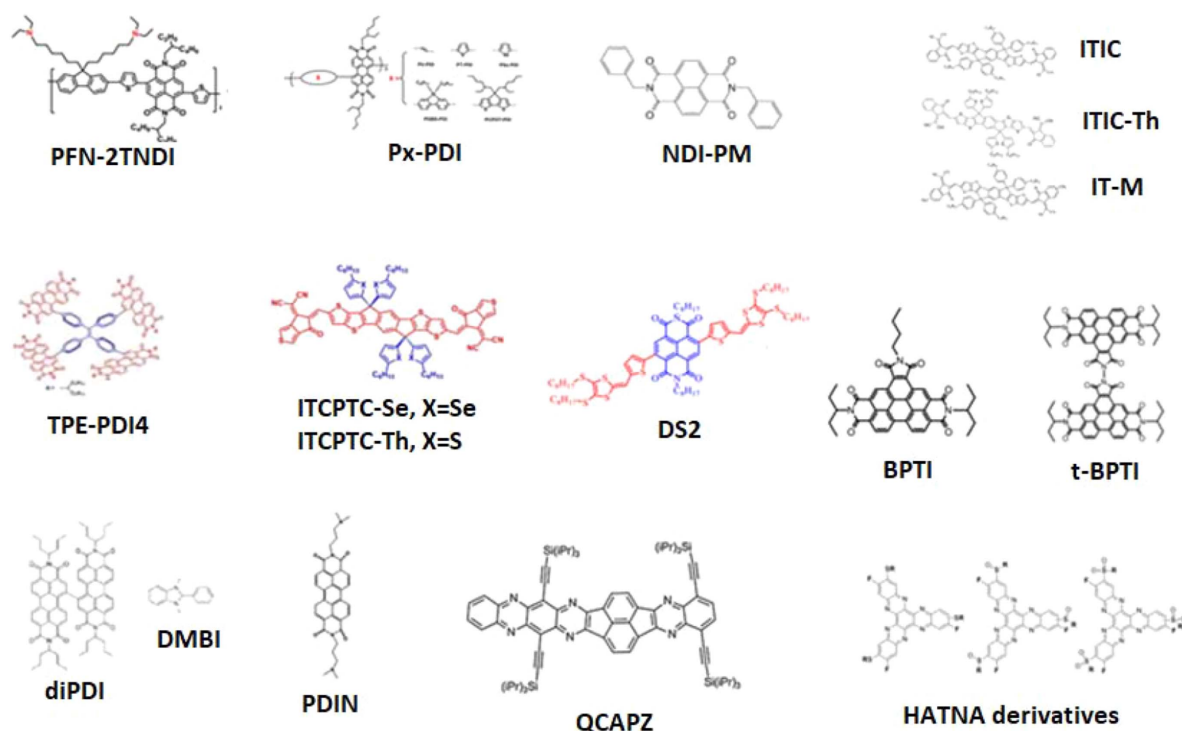


Figure 14. Chemical structures of non-fullerene materials used as ETLs in OSCs and PeSCs.

suggested a better contact between the ETL and the underlying perovskite layer facilitating charge transfer. The reduction in the hysteresis index (HI) plays a critical role in the performance of the PeSCs. Jian Zhang's group [239] introduced three non-fullerene acceptors, ITIC, ITIC-Th, and IT-M as ETLs in inverted PeSCs. The hysteresis indexes of the ITIC, ITIC-Th, and IT-M based devices were 1.78, 1.35, and 1.83, respectively, compared to the PCBM-based device which was 3.37. These results were attributed to the smooth film morphology, the reduction of recombination losses and the passivation of the photoactive layer. Besides using non-fullerene materials as ETLs, some groups also attempted to either dope them or appropriately combine them. Ho Jo *et al* [240] incorporated a perylene diimide dimer (diPDI) as ETL in inverted PeSCs. The diPDI-based devices achieved a PCE of 7.1%. When the diPDI was n-doped with DMBI, the PCE was increased to 10.0%. The doping caused an up-shifting of the Fermi level of the diPDI from 4.95 eV to 4.71 eV, enhancing electron transport. Moreover, Chu's group [241] combined benzo[ghi]perylene triimide (BPTI) and one derivative (t-BPTI) as ETLs in inverted PeSCs. An improved performance, as well as reduced hysteresis, was achieved for the non-fullerene devices. Furthermore, Meng's group [242] demonstrated that a perylene derivative (PDIN) can be dissolved in 2,2,2-trifluoroethanol, forming a high-quality film atop the perovskite layer and also overcoming the erosion problem of conventional alcohol solvents.

Apart from PDI and NDI derivatives, other non-fullerene small molecules can be used as ETLs. Marder *et al* [243] introduced the use of the small molecule hexaazatrinaphthylene (HATNA) with comparable characteristics with the

fullerene materials. However, some obstacles such as poor solubility need to be overcome. Jen's group replaced three F groups of HATNA-F₆ with three alkylsulfanyl chains of different lengths. The HATNA derivative-based PeSCs showed a PCE of 17.6%. In addition, QCAPZ (1,4,9,16-tetrakis ((triisopropylsilyl)ethynyl) quinoxalino [200 0,300 0:400 500] cyclopenta [100 200 300:50,60] acenaphtho[10,20:5,6] pyrazino[2,3-b]phenazine), one azacene derivative presented by Zhang's group [244] as an alternative non-fullerene ETL in PeSCs, exhibited an improved performance. Figure 14 presents the chemical structures of some non-fullerene materials used as ETLs in OSCs and PeSCs.

HATNA derivatives (HATNA-F₆, and HATNA-F₁₂) were also employed as ETLs in OSCs to replace the C₆₀, due to their attractive characteristics (large optical bandgap, low surface roughness, sufficiently high electron mobility) leading to an increase in the OSCs' performance [245]. Very recently, Yella's group [246] employed ITIC in inverted OSCs to modify the ZnO/photoactive layer interface. It was found that the PCE was increased from 7.5% for the reference device to 9% for the OSC with the ITIC interlayer, attributed to the improvement in the quality of the ZnO/active layer interface.

4.2. Inorganic molecular electron transport materials

4.2.1. Polyoxometalates.

Solution-processed POMs, which have long been considered as effective electron mediators and have tunable metal-derived LUMO levels, have been employed as alternative ETLs and cathode interlayers in both regular- and inverted-architecture OSCs and PeSCs at an increasing rate in the last few years. Since the first successful

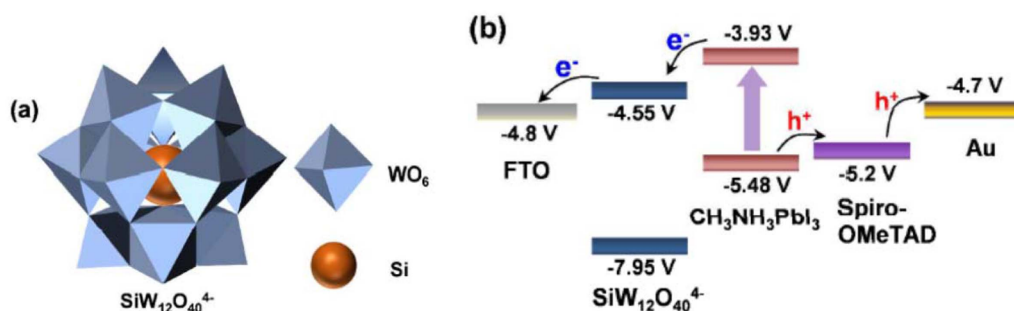


Figure 15. (a) Crystal structure of $\text{SiW}_{12}\text{O}_{40}^{4-}$ POM. (b) Energy level diagram of perovskite solar cells employing $\text{SiW}_{12}\text{O}_{40}^{4-}$ as an ETL. Reprinted with permission from [257]. Copyright (2018) American Chemical Society.

demonstration of a water-soluble Keggin-type W-based POM ($\text{iH}_3\text{PW}_{12}\text{O}_{40}$) as an effective ETL in P3HT:PCBM-based OSCs [247], which improved both its PCE and its shelf storage stability in ambient conditions, other POMs have been incorporated as highly effective ETLs or in combination with TiO_2 and ZnO in both OSCs and PeSCs. Notable cases include Keggin POMs $\text{H}_4\text{SiW}_{12}\text{O}_{40}$, $\text{H}_3\text{PW}_{12}\text{O}_{40}$ and $\text{H}_3\text{PMo}_{12}\text{O}_{40}$, the mixed addenda $\text{H}_5\text{PV}_2\text{W}_{10}\text{O}_{40}$, the Dawson POMs $(\text{NH}_4)_6\text{P}_2\text{W}_{18}\text{O}_{62}$ and $(\text{NH}_4)_6\text{P}_2\text{Mo}_{18}\text{O}_{62}$ [248], lacunary-type POMs such as $(\text{nBu}_4\text{N})_3[\text{PW}_9\text{O}_{34}(\text{tBuSiOH})_3]$ [249], silanol-functionalized POMs [250] and surfactant-encapsulated POMs such as $[(\text{C}_8\text{H}_{17})_4\text{N}]_4[\text{SiW}_{12}\text{O}_{40}]$ [251, 252]. For example, optimized POM-modified PTB7:PCBM- and PTB7-Th:PC₇₁BM-based OSCs exhibited efficiencies of 8.07% and 10.1% respectively (an 11% and 21% respective enhancement compared to the reference cells) by simultaneously improving the cells' V_{oc} , J_{sc} , and FF. Successful incorporation of different POMs as ETLs in other types of solar cells was recently expanded in the fast-growing field of PeSCs with excellent results demonstrated by various groups [253, 257]. Figure 15 shows a representative example of a $\text{SiW}_{12}\text{O}_{40}^{4-}$ Keggin POM which was used as a sole ETL in $\text{CH}_3\text{NH}_3\text{PbI}_3$ -based PeSCs along with the corresponding cell energy level, resulting in significant improvements (>20%) in cell PCE and stability.

The improvements in PCE and long-term storage and photostability were generally attributed to enhanced electron transfer/extraction and reduced recombination losses at the POM-modified cathode interface as a result of the favorable energy level alignment and the lower electron extraction barrier, POM reduction upon contact with Al (depending on the position of their LUMO level) [258], and the high ability of POMs to act as efficient oxygen radical scavengers. Upon coating ZnO and TiO_2 with a thin POM overlayer, an effective oxide passivation and a decrease in oxides' surface energy were also observed which synergistically resulted in a superior electron transfer capability of the functionalized oxide/POM interface.

4.2.2. Ionic liquids. Ionic liquids (ILs) have gained the interest of researchers for their unique properties that make them suitable as interfacial layers in OSCs and PeSCs. In particular, their exceptional electrochemical and thermal stability, high electron mobility, large ionic conductivity, as well as

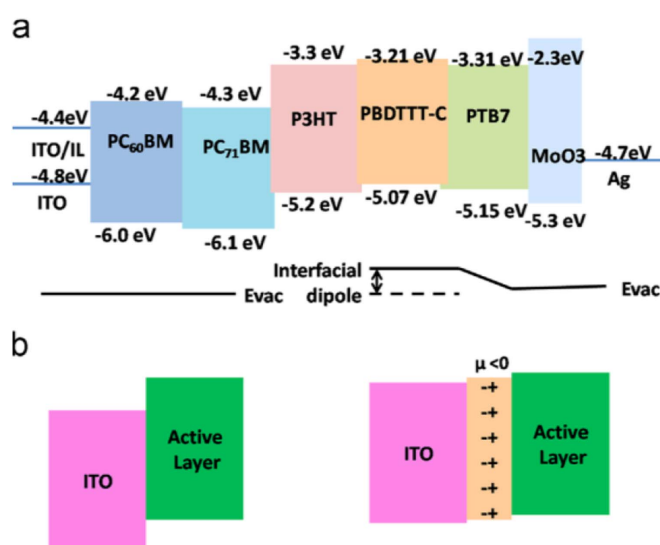


Figure 16. (a) Energy level diagram of the polymers and BenMeIm-Cl IL components used in the IPSCs. (b) Illustration of vacuum-level shift and reduced work function of ITO after deposition of the BenMeIm-Cl IL layer. Reprinted from [262]. Copyright (2015), with permission from Elsevier.

their beneficial hydrophilic nature and superior transmittance make ILs promising materials to enhance electron transport/extraction when inserted between the photoactive layer and the cathode of the OSCs and/or PeSCs. Lee *et al* [259] investigated the surface modification of ZnO using ionic liquids in hybrid polymeric solar cells. It is observed that 1-benzyl-3-methylimidazolium chloride (benmim-Cl) improved the device performance, which was attributed to the enhanced electron transfer at the ZnO /active layer interface, ascribed to the effective ionic dipole polarization. In another study, Zhu and coworkers [260] used ionic liquid-functionalized carbon nanoparticles (ILCNs) as modifiers of the electron-selective ZnO layer in inverted polymer solar cells. ILCN-modified ZnO ETL improved the interfacial contact between the ZnO and the active layer (P3HT:PCBM), and thus the device performance, exhibiting a 29.8% increase in the PCE value, compared with that of the pristine ZnO -based inverted OSC. Furthermore, Li's group [261] demonstrated the influence of the interfacial layer on the performance of inverted OSCs when a ZnO /ionic liquid ETL was employed at the cathode/active

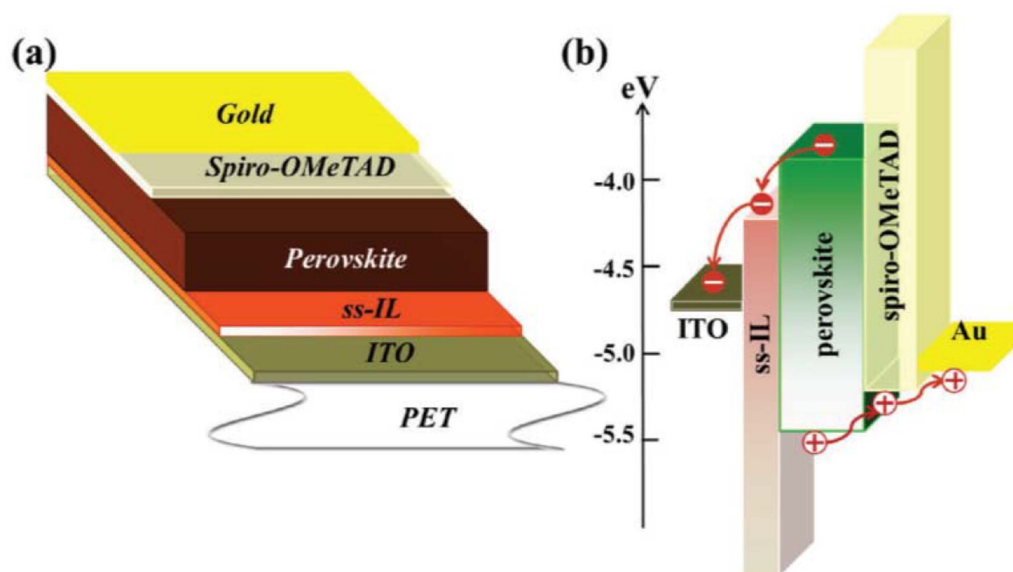


Figure 17. (a) Structure of the flexible PeSC with ss-IL as the ETM. (b) Energy level diagram of the PeSC, exhibiting the collecting process of photogenerated charge carriers. [264] John Wiley & Sons. Copyright (2016) WILEY-VCH Verlag GmbH & Co. KGaA, Weinheim.

layer interface. OSCs using the $\text{ZnO}/[\text{BMIM}]\text{BF}_4$ (1-butyl-3-methylimidazolium tetrafluoroborate) achieved a high PCE value of 10.15%, which was among the highest efficiencies reported at that time for a single-junction OSC. The introduced IL reduced the W_F of the ZnO/IL substrate, leading to improved electron extraction. Fu *et al* [262] have extended the application of ILs, used as an independent cathode interfacial layer in inverted OSCs (figure 16). The inserted BenMeIm-Cl ionic liquid between the ITO and the photoactive blend layer facilitated the electron transport, attributed to the dipolar polarization at the ITO/photoactive layer interface. Consequently, well-matched energy levels were observed, resulting in increased PCE values for the IL-based devices. In order to investigate the role of cations and substituents of ILs on the OSCs' performance, Yu *et al* [263] used three ILs based on different cations and invariable anion BF_4^- as a replacement for Ca in forward-configuration OSCs. IL layers incorporated between the photoactive layer and the cathode reduced the series resistance of the OSC, as well as the electron extraction barrier at the same interface. In addition, an increase in electron mobility was observed, facilitating electron transport and thus resulting in improved device performance. It was also found that the type of cation is critical for the device efficiency, since alkyl-containing IL-based OSCs exhibited higher PCE values (7.29%) than those with heterocyclic counterparts (5.88%).

Recently, ILs have been successfully used as interfacial layers in PeSCs. Yang and co-workers [264] employed 1-benzyl-3-methylimidazolium chloride solid-state ionic liquid (ss-IL) $[\text{BMIM}]\text{Cl}$ via solution processing as an effective ETL in flexible PeSCs (figure 17). The device with the ss-IL exhibited a higher PCE value of 15.04%, compared to the reference one without the ETL, attributed to the facile electron transfer from the perovskite absorber towards the selective contact electrode. The introduced ss-IL as an ETL reduced

the W_F of ITO, leading to high electron mobility values, which also improved the device FF and J_{sc} and thus the PeSC performance. In addition, ss-IL substrates influenced the nano-morphology of the perovskite absorber coated on top of them, since the hydrophilicity of the ss-IL was beneficial to the perovskite film formation, resulting in a smoother film surface. The ss-IL also reduced the electron trap-state density, leading to the suppression of the undesirable hysteresis of the PeSCs. In another work, Yang *et al* [265] demonstrated the use of an ionic liquid, in particular 1-butyl-3-methylimidazolium tetrafluoroborate $[\text{BMIM}]\text{BF}_4$, as a surface modifier of TiO_2 ETL applied in planar-configuration PeSCs. The IL-modified TiO_2 -based PeSC achieved a large PCE value of 19.62%, the highest recorded PCE value for planar perovskite solar cells at that time, also showing almost no hysteresis. This remarkable enhancement of device performance was mainly attributed to the improved electron mobility and reduced W_F of IL-modified TiO_2 , leading to well-matched energy levels with that of the perovskite absorber. Also, the IL modifier suppressed charge accumulation resulting in increased device stability. Moreover, Yang's group [266] studied two ionic liquids with different ions as both independent ETL and TiO_2 modifiers in planar PeSCs based on MAPbI_3 . It has been demonstrated that the device with the IL 1-methylimidazolium iodide $[\text{EMIM}]\text{I}$ used as an independent ETL showed low performance (PCE value of 9.17%) attributed to the poor film formation of $[\text{EMIM}]\text{I}$ on top of the FTO substrates, resulting in direct contact between the perovskite absorber and the cathode. On the other hand, the PeSCs based on $[\text{EMIM}]\text{I}$ -modified TiO_2 ETL exhibited a higher PCE value of 18.08% when compared with the reference device. Therefore, it was suggested that $[\text{EMIM}]^+$ anions have a significant impact on the electron transport ability of independent IL on FTO substrates, while they affect the electron transport of IL-modified TiO_2 ETLs less when $[\text{EMIM}]\text{I}$ is coated on them. In the same

work, the application of [EMIM]PF₆ was also investigated as an independent ETL and TiO₂ modifier. The PeSC with the IL-modified TiO₂ exhibited a PCE value of 19.59%, while the device based on the independent [EMIM]PF₆ ETL showed a PCE of 14.39%. The introduced IL was beneficial to the crystallinity and film coverage of the perovskite absorber, leading to improved electron transport between the active layer and the selective electrode, as well as reduced recombination losses at the perovskite/ETL interface.

Recently, ionic liquids have been also used as ZnO modifiers in planar-configuration perovskite solar cells, leading to effective interface passivation and enhanced long-term device stability. In particular, Zhang *et al* [267] employed [EMIM]PF₆ between the ZnO ETL and the MAPbI₃ perovskite film, achieving a highly efficient and chemical stable device. The performance of the IL-modified ZnO-based PeSC was increased by over 25% compared with the pristine device, which was attributed to the effective passivation effect of the [EMIM]PF₆, and thus the enhanced electron transport ability of the ZnO ETL. In addition, the applied IL on ZnO improved perovskite film formation, while also preventing the penetration of moisture into the device, quenching the degradation of the perovskite film, resulting in long-term stable PeSCs with small hysteresis. Subsequently, Chu and co-workers [268] also investigated the effect of IL modification at the ZnO/MAPbI₃ interface in flexible PeSCs. The employed [BMIM]BF₄ improved the ZnO ETL film formation, enhanced the crystallinity of the perovskite absorber coated on it, and thus increased the electron extraction. Consequently, the PCE value of the IL-modified ZnO-based device increased by 1.4 times compared to the PeSC with the pristine ZnO ETL. Recently, Huang *et al* [269] studied the effect of SnO₂ modification used as an ETL in perovskite solar cells by inserting the IL tetramethylammonium hydroxide (TMAH) into SnO₂ nanoparticle suspension. Interestingly, the TMAH-modified SnO₂ ETLs showed improved conductivity, while effective passivation at the perovskite surface and grain boundaries observed enhanced electron transport from the active layer to the selective contact electrode. As a result, highly efficient PeSCs based on the TMAH-modified SnO₂ ETL were achieved with PCE values over 20%, also exhibiting outstanding device stability. Despite the fact that SnO₂ is less defective compared to ZnO and TiO₂ has demonstrated high PeSCs efficiencies in its pristine form [270, 271], the application of surface modifiers may push these oxide capabilities further.

Furthermore, Yao's group [272] demonstrated the benefits of ssILs as a bilayer ETL (ss-IL/C₆₀) in n-i-p planar-heterojunction PeSCs. It is reported that upon [EMIM]I application the W_F of FTO was reduced, leading to a more favorable energy level alignment at the ETL/perovskite interface. In addition, the uniform and smooth film formation of the active layer, attributed to the hydrophilicity of the IL, resulted in reduced defect density and improved device stability. The fabricated PeSCs using the [EMIM]I ETL also exhibited high performance with a PCE value of 15.09% compared with the device based on the unmodified ETL. In a recent work, Li *et al* [273] studied the influence of ionic liquids on the performance of inverted PeSCs employed

at the PCBM/electrode interface. In particular, the use of [BMIM]BF₄ increased device efficiency up to 19.3%, attributed to the facile electron transport/extraction and efficient surface passivation of PCBM film. The IL film also prolonged the PeSCs' stability, playing the role of a protective layer and preventing moisture and oxygen from penetrating into the perovskite film.

5. Summary and outlook

In this review we summarize recent reports on the development/synthesis of novel molecular materials, either organic or inorganic, for interface engineering in organic and perovskite solar cells. A vast variety of molecular materials have recently been designed and synthesized with the aim of serving as efficient hole or electron transport layers. Their role is to enhance the charge transport/extraction towards the respective electrodes, hence improving the overall device performance. Despite the significant progress, further efforts are needed to design and synthesize multifunctional molecular materials with excellent optoelectronic properties and cost-effectiveness for sophisticated device engineering. Such materials could contribute to simplified, low-cost device architecture that is a prerequisite for future commercialization. Based on this review, guidance for designing and applying new organic interfacial materials can be formulated as follows.

- (a) Use careful design of new types of molecular materials possessing high charge carrier mobility, suitable energy levels, hydrophobicity, good solubility, and low cost.
- (b) Introduction of suitable functional groups (such as amines) onto the surface of organic interfacial materials is beneficial for facilitating charge carrier extraction or injection.
- (c) Increasing the hydrophobicity of molecular interfacial materials can protect the active layer from moisture, improving long-term stability.
- (d) Easily synthesized, cost-effective and high-yield molecular materials for OSCs and PeSCs are highly desirable.
- (e) Pursuit of materials that play multifunctional roles when applied in the complete device.

We anticipate that with strong collaboration between chemistry, materials science and device physics, significant progress in the development of such molecular materials will be achieved in the near future.

Acknowledgments

Support of this work by the project 'Development of Materials and Devices for Industrial, Health, Environmental and Cultural Applications' (MIS 5002567) which is implemented under the 'Action for the Strategic Development on the Research and Technological Sector', funded by the Operational Programme 'Competitiveness, Entrepreneurship and Innovation' (NSRF 2014-2020) and co-financed by Greece and the European Union (European Regional Development Fund), is acknowledged.

ORCID iDs

Anastasia Soultati  <https://orcid.org/0000-0001-6683-6810>

Kalliopi Ladomenou  <https://orcid.org/0000-0002-8508-1369>

Maria Vasilopoulou  <https://orcid.org/0000-0001-8893-1691>

References

- [1] Zhao J *et al* 2015 High-efficiency non-fullerene organic solar cells enabled by a difluorobenzothiadiazole-based donor polymer combined with a properly matched small molecule acceptor *Energy Environ. Sci.* **8** 520–5
- [2] Forrest S R 2004 The path to ubiquitous and low-cost organic electronic appliances on plastic *Nature* **428** 911–8
- [3] He Z, Xiao B, Liu F, Wu H, Yang Y, Xiao S, Wang C, Russell T P and Cao Y 2015 Single-junction polymer solar cells with high efficiency and photovoltage *Nat. Photon.* **9** 174–9
- [4] Lai T H, Tsang S W, Manders J R, Chen S and So F 2013 Properties of interlayer for organic photovoltaics *Mater. Today* **16** 424–32
- [5] Liu Y, Zhao J, Li Z, Mu C, Ma W, Hu H, Jiang K, Lin H, Ade H and Yan H 2014 Aggregation and morphology control enables multiple cases of high-efficiency polymer solar cells *Nat. Commun.* **5** 1–8
- [6] Zhao W, Li S, Yao H, Zhang S, Zhang Y, Yang B and Hou J 2017 Molecular optimization enables over 13% efficiency in organic solar cells *J. Am. Chem. Soc.* **139** 7148–51
- [7] Lee W, Jeong S, Lee C, Han G, Cho C, Lee J Y and Kim B J 2017 Self-organization of polymer additive, poly(2-vinylpyridine) via one-step solution processing to enhance the efficiency and stability of polymer solar cells *Adv. Energy Mater.* **7** 1602812
- [8] Liu J *et al* 2016 Fast charge separation in a non-fullerene organic solar cell with a small driving force *Nat. Energy* **1** 1–7
- [9] Cui Y *et al* 2019 Over 16% efficiency organic photovoltaic cells enabled by a chlorinated acceptor with increased open-circuit voltages *Nat. Commun.* **10** 2515
- [10] Meng L *et al* 2018 Organic and solution-processed tandem solar cells with 17.3% efficiency *Science* **361** 1094–8
- [11] Yang W S, Noh J H, Jeon N J, Kim Y C, Ryu S, Seo J and Seok S I 2015 High-performance photovoltaic perovskite layers fabricated through intramolecular exchange *Science* **348** 1234–7
- [12] Fabiani D H, Stoumpos C C, Laurita G, Kaltzoglou A, Kontos A G, Falaras P, Kanatzidis M G and Seshadri R 2016 Reentrant structural and optical properties and large positive thermal expansion in perovskite formamidinium lead iodide *Angew. Chem., Int. Ed.* **55** 15392–6
- [13] Lee M M, Teuscher J, Miyasaka T, Murakami T N and Snaith H J 2012 Efficient hybrid solar cells based on meso-superstructured organometal halide perovskites *Science* **338** 643–8
- [14] Christians J A, Miranda Herrera P A and Kamat P V 2015 Transformation of the excited state and photovoltaic efficiency of CH₃NH₃PbI₃ perovskite upon controlled exposure to humidified air *J. Am. Chem. Soc.* **137** 1530–8
- [15] Chen W *et al* 2015 Efficient and stable large-area perovskite solar cells with inorganic charge extraction layers *Science* (80-.) **350** 944–8
- [16] Liu M, Johnston M B and Snaith H J 2013 Efficient planar heterojunction perovskite solar cells by vapour deposition *Nature* **501** 395–8
- [17] Kuang C *et al* 2015 Highly efficient electron transport obtained by doping PCBM with graphdiyne in planar-heterojunction perovskite solar cells *Nano Lett.* **15** 2756–62
- [18] Zhou H, Chen Q, Li G, Luo S, Song T-B, Duan H-S, Hong Z, You J, Liu Y and Yang Y 2014 Interface engineering of highly efficient perovskite solar cells *Science* **345** 542
- [19] Wu Z, Wu B, Tam H L and Zhu F 2016 An insight on oxide interlayer in organic solar cells: from light absorption and charge collection perspectives *Org. Electron.* **31** 266–72
- [20] Facchetti A 2013 Polymer donor–polymer acceptor (all-polymer) solar cells *Mater. Today* **16** 123–32
- [21] Vasilopoulou M, Soultati A, Georgiadou D G, Stergiopoulos T, Palilis L C, Kennou S, Stathopoulos N A, Davazoglou D and Argitis P 2014 Hydrogenated under-stoichiometric tungsten oxide anode interlayers for efficient and stable organic photovoltaics *J. Mater. Chem. A* **2** 1738–49
- [22] Vasilopoulou M *et al* 2012 The influence of hydrogenation and oxygen vacancies on molybdenum oxides work function and gap states for application in organic optoelectronics *J. Am. Chem. Soc.* **134** 16178–87
- [23] Wang F, Tan Z and Li Y 2015 Solution-processable metal oxides/chelates as electrode buffer layers for efficient and stable polymer solar cells *Energy Environ. Sci.* **8** 1059–91
- [24] Wang H-Q, Li N, Guldal N S and Brabec C J 2012 Nanocrystal V₂O₅ thin film as hole-extraction layer in normal architecture organic solar cells *Org. Electron.* **13** 3014–21
- [25] Vasilopoulou M *et al* 2014 Atomic-layer-deposited aluminum and zirconium oxides for surface passivation of TiO₂ in high-efficiency organic photovoltaics *Adv. Energy Mater.* **4** 1400214
- [26] Raptis I, Velessiotis D, Vasilopoulou M and Argitis P 2000 Development mechanism study by dissolution monitoring of positive methacrylate photoresists *Microelectron. Eng.* **53** 489–92
- [27] Li N, McCulloch I and Brabec C J 2018 Analyzing the efficiency, stability and cost potential for fullerene-free organic photovoltaics in one figure of merit *Energy Environ. Sci.* **11** 1355–61
- [28] Polydorou E *et al* 2017 Avoiding ambient air and light induced degradation in high-efficiency polymer solar cells by the use of hydrogen-doped zinc oxide as electron extraction material *Nano Energy* **34** 500–14
- [29] Lange I *et al* 2014 Tuning the work function of polar zinc oxide surfaces using modified phosphonic acid self-assembled monolayers *Adv. Funct. Mater.* **24** 7014–24
- [30] Vasilopoulou M 2014 The effect of surface hydrogenation of metal oxides on the nanomorphology and the charge generation efficiency of polymer blend solar cells *Nanoscale* **6** 13726–39
- [31] Habisreutinger S N, Leijtens T, Eperon G E, Stranks S D, Nicholas R J and Snaith H J 2014 Carbon nanotube/polymer composites as a highly stable hole collection layer in perovskite solar cells *Nano Lett.* **14** 5561–8
- [32] Intemann J J *et al* 2014 Highly efficient inverted organic solar cells through material and interfacial engineering of indacenodithieno[3,2-b]thiophene-based polymers and devices *Adv. Funct. Mater.* **24** 1465–73
- [33] Lim K G, Choi M R and Lee T W 2017 Improvement of both efficiency and stability in organic photovoltaics by using water-soluble anionic conjugated polyelectrolyte interlayer *Mater. Today Energy* **5** 66–71
- [34] Seo J H, Gutacker A, Sun Y, Wu H, Huang F, Cao Y, Scherf U, Heeger A J and Bazan G C 2011 Improved high-efficiency organic solar cells via incorporation of a conjugated polyelectrolyte interlayer *J. Am. Chem. Soc.* **133** 8416–9

- [35] Gogolides E, Argitis P, Couladouros E A, Vidali V P, Vasilopoulou M and Cordoyiannis C 2005 Polycarbocyclic derivatives for modification of resist, optical and etch resistance properties *US Patent* 1444550
- [36] Yu J, Xi Y, Chueh C C, Xu J Q, Zhong H, Lin F, Jo S B, Pozzo L D, Tang W and Jen A K Y 2017 Boosting performance of inverted organic solar cells by using a planar coronene based electron-transporting layer *Nano Energy* **39** 454–60
- [37] Gu C, Zhang Z, Sun S, Pan Y, Zhong C, Lv Y, Li M, Ariga K, Huang F and Ma Y 2012 In situ electrochemical deposition and doping of C₆₀ films applied to high-performance inverted organic photovoltaics *Adv. Mater.* **24** 5727–31
- [38] Zhang Z G, Qi B, Jin Z, Chi D, Qi Z, Li Y and Wang J 2014 Perylene diimides: a thickness-insensitive cathode interlayer for high performance polymer solar cells *Energy Environ. Sci.* **7** 1966–73
- [39] Pho T V, Kim H, Seo J H, Heeger A J and Wudl F 2011 Quinacridone-based electron transport layers for enhanced performance in bulk-heterojunction solar cells *Adv. Funct. Mater.* **21** 4338–41
- [40] Lee H, Puodziukynaite E, Zhang Y, Stephenson J C, Richter L J, Fischer D A, Delongchamp D M, Emrick T and Briseno A L 2015 Poly(sulfobetaine methacrylate)s as electrode modifiers for inverted organic electronics *J. Am. Chem. Soc.* **137** 540–9
- [41] Nian L, Zhang W, Wu S, Qin L, Liu L, Xie Z, Wu H and Ma Y 2015 Perylene bisimide as a promising zinc oxide surface modifier: enhanced interfacial combination for highly efficient inverted polymer solar cells *ACS Appl. Mater. Interfaces* **7** 540–9
- [42] Sun K, Zhao B, Murugesan V, Kumar A, Zeng K, Subbiah J, Wong W W H, Jones D J and Ouyang J 2012 High-performance polymer solar cells with a conjugated zwitterion by solution processing or thermal deposition as the electron-collection interlayer *J. Mater. Chem.* **22** 24155–65
- [43] Jia T, Zhou W, Chen Y, Han J, Wang L, Li F and Wang Y 2015 Highly efficient polymer solar cells based on a universal cathode interlayer composed of metallophthalocyanine derivative with good film-forming property *J. Mater. Chem. A* **3** 4547–54
- [44] Umari P, Mosconi E and De Angelis F R G 2014 Calculations on CH₃NH₃PbI₃ and CH₃NH₃SnI₃ perovskites for solar cell applications *Sci. Rep.* **4** 4467
- [45] Jena A K, Kulkarni A and Miyasaka T 2019 Halide perovskite photovoltaics: background, status, and future prospects *Chem. Rev.* **119** 3036–103
- [46] Ava T T, Al Mamun A, Marsillac S and Namkoong G 2019 A review: thermal stability of methylammonium lead halide based perovskite solar cells *Appl. Sci.* **9** 188
- [47] Li H, Xiao Z, Ding L and Wang J 2018 Thermostable single-junction organic solar cells with a power conversion efficiency of 14.62% *Sci. Bull.* **63** 340–2
- [48] Xiong J, Jin K, Qin J *et al* 2019 Thiolactone copolymer donor gifts organic solar cells a 16.72% efficiency *Sci. Bull.* **64** 1573–6
- [49] Jiang Q, Chu Z, Wang P, Yang X, Liu H, Wang Y, Yin Z, Wu J, Zhang X and You J 2017 Planar-structure perovskite solar cells with efficiency beyond 21% *Adv. Mater.* **29** 1703852
- [50] Jiang Q, Zhao Y, Zhang X, Chen Y, Chu Z, Ye Q, Li X, Yin Z and You J 2019 Surface passivation of perovskite film for efficient solar cells *Nat. Photon.* **13** 460–6
- [51] Huang J-S, Chou C-Y, Liu M-Y, Tsai K-H, Lin W-H and Lin C-F 2009 Solution-processed vanadium oxide as an anode interlayer for inverted polymer solar cells hybridized with ZnO nanorods *Org. Electron.* **10** 1060–5
- [52] Hwang H, Park S, Heo J H, Kim W, Ahn H, Kim T S, Im S H and Son H J 2019 Enhancing performance and stability of perovskite solar cells using hole transport layer of small molecule and conjugated polymer blend *J. Power Sources* **418** 167–75
- [53] Chien H T, Pilat F, Griesser T, Fizek H, Poelt P and Friedel B 2018 Influence of environmentally affected hole-transport layers on spatial homogeneity and charge-transport dynamics of organic solar cells *ACS Appl. Mater. Interfaces* **10** 10102–14
- [54] Liu B *et al* 2019 Boosting efficiency and stability of organic solar cells using ultralow-cost BiOCl nanoplates as hole transporting layers *ACS Appl. Mater. Interfaces* **11** 33505–14
- [55] Soultati A *et al* 2014 Solution-processed hydrogen molybdenum bronzes as highly conductive anode interlayers in efficient organic photovoltaics *Adv. Energy Mater.* **4** 1300896
- [56] Bai Y *et al* 2016 Effects of a molecular monolayer modification of NiO nanocrystal layer surfaces on perovskite crystallization and interface contact towards faster hole extraction and higher photovoltaic performance *Adv. Funct. Mater.* **26** 2950–8
- [57] Galatopoulos F, Savva A, Papadas I T and Choulis S A 2017 The effect of hole transporting layer in charge accumulation properties of p-i-n perovskite solar cells *APL Mater.* **5** 076102
- [58] Widjonarko N E *et al* 2014 Impact of hole transport layer surface properties on the morphology of a polymer–fullerene bulk heterojunction *Adv. Energy Mater.* **4** 1301879
- [59] Li Q, Sun Y, Yang C, Liu K, Islam M R, Li L, Wang Z and Qu S 2019 Optimizing the component ratio of PEDOT:PSS by water rinse for high efficiency organic solar cells over 16.7% *Sci. Bull.* (in press)
- [60] Sun Y, Yang C, Li Q, Liu K *et al* 2020 The route and optimization of charge transport in ternary organic solar cells based on O6T-4F and PC71BM as acceptors *J. Power Sources* **449** 227583
- [61] Calió L, Kazim S, Grätzel M and Ahmad S 2016 Hole-transport materials for perovskite solar cells *Angew. Chem., Int. Ed.* **55** 14522–45
- [62] Yu Z and Sun L 2015 Recent progress on hole-transporting materials for emerging organometal halide perovskite solar cells *Adv. Energy Mater.* **5** 1500213
- [63] Gheno A, Vedraïne S, Ratier B and Bouclé J 2016 π -conjugated materials as the hole-transporting layer in perovskite solar cells *Metals (Basel)* **6** 21
- [64] Vivo P, Salunke J K and Priimagi A 2017 Hole-transporting materials for printable perovskite solar cells *Materials (Basel)* **10** 1–45
- [65] Heo J H *et al* 2013 Efficient inorganic–organic hybrid heterojunction solar cells containing perovskite compound and polymeric hole conductors *Nat. Photon.* **7** 486–91
- [66] Agarwala P and Kabra D 2017 A review on triphenylamine (TPA) based organic hole transport materials (HTMs) for dye sensitized solar cells (DSSCs) and perovskite solar cells (PSCs): evolution and molecular engineering *J. Mater. Chem. A* **5** 1348–73
- [67] Green M A, Hishikawa Y, Dunlop E D, Levi D H, Hohl-Ebinger J and Ho-Baillie A W Y 2018 Solar cell efficiency tables (version 51) *Prog. Photovolt., Res. Appl.* **26** 3–12
- [68] Liu Y, Zuo Y, Li S, Li J, Li L, Liu C, Ashraf S, Li P and Wang B 2019 Synthesis and fine-tuning the pore properties of a thiophene based porous organic framework by post-oxidation treatment *J. Mater. Chem. A* **7** 21953–8
- [69] Tlach B C, Tomlinson A L, Bhuwalka A and Jeffries-El M 2011 Tuning the optical and electronic properties of

- 4,8-disubstituted benzobisoxazoles via alkyne substitution *J. Org. Chem.* **76** 8670–81
- [70] Wazzan N and Safi Z 2019 Effect of number and position of methoxy substituents on fine-tuning the electronic structures and photophysical properties of designed carbazole-based hole-transporting materials for perovskite solar cells: DFT calculations *Arab. J. Chem.* **12** 1–20
- [71] Chen R, Lu R Q, Shi P C and Cao X Y 2016 Corannulene derivatives for organic electronics: from molecular engineering to applications *Chin. Chem. Lett.* **27** 1175–83
- [72] Steirer K X, Chesin J P, Widjonarko N E, Berry J J, Miedaner A, Ginley D S and Olson D C 2010 Solution deposited NiO thin-films as hole transport layers in organic photovoltaics *Org. Electron.* **11** 1414–8
- [73] Inzani K, Nematollahi M, Selbach S M, Grande T, Waalekalv M L, Brakstad T, Reenaas T W, Kildemo M and Vullum-Bruer F 2018 Tailoring properties of nanostructured MoO_{3-x} thin films by aqueous solution deposition *Appl. Surf. Sci.* **459** 822–9
- [74] Manders J R, Tsang S, Hartel M J, Lai T, Chen S, Amb C M, Reynolds J R and So F 2013 Solution-processed nickel oxide hole transport layers in high efficiency polymer photovoltaic cells *Adv. Funct. Mater.* **23** 2993–3001
- [75] Li X, Zhang W, Wu Y, Min C and Fang J 2013 Solution-processed MoS_x as an efficient anode buffer layer in organic solar cells *ACS Appl. Mater. Interfaces* **5** 8823–7
- [76] Treat N D, Yaacobi-Gross N, Faber H, Perumal A K, Bradley D D C, Stingelin N and Anthopoulos T D 2015 Copper thiocyanate: an attractive hole transport/extraction layer for use in organic photovoltaic cells *Appl. Phys. Lett.* **107** 013301
- [77] Wijeyasinghe N, Regoutz A, Eisner F Du T *et al* 2017 Copper(I) thiocyanate (CuSCN) hole-transport layers processed from aqueous precursor solutions and their application in thin-film transistors and highly efficient organic and organometal halide perovskite solar cells *Adv. Funct. Mater.* **27** 1701818
- [78] Arora H, Dar M I, Hinderhofer A, Pellet N, Schreiber F, Zakeeruddin S M and Grätzel M 2017 Perovskite solar cells with CuSCN hole extraction layers yield stabilized efficiencies greater than 20% *Science* **358** 768–71
- [79] Wijeyasinghe N, Eisner F, Tsetseris L Lin Y-H *et al* 2018 p-doping of copper(I) thiocyanate (CuSCN) hole-transport layers for high-performance transistors and organic solar cells *Adv. Funct. Mater.* **28** 1802055
- [80] Jin I S, Lee J H, Noh Y W, Park S H and Jung J W 2019 Molecular doping of CuSCN for hole transporting layers in inverted-type planar perovskite solar cells *Inorg. Chem. Front.* **6** 2158–66
- [81] Wang H, Yu Z, Lai J, Song X, Yang X, Hagfeldt A and Sun L 2018 One plus one greater than two: high-performance inverted planar perovskite solar cells based on a composite CuI/CuSCN hole-transporting layer *J. Mater. Chem. A* **6** 21435–44
- [82] Zhu Y, Yuan Z, Cui W, Wu Z, Sun Q, Wang S, Kang Z and Sun B 2014 A cost-effective commercial soluble oxide cluster for highly efficient and stable organic solar cells *J. Mater. Chem. A* **2** 1436–42
- [83] Vasilopoulou M, Polydorou E, Douvas A M, Palilis L C, Kennou S and Argyitis P 2015 Annealing-free highly crystalline solution-processed molecular transition metal oxides as charge transport and recombination layers for efficient and stable single-junction and tandem polymer solar cells *Energy Environ. Sci.* **8** 2448–63
- [84] Aizawa N, Fuentes-Hernandez C, Kolesov V A, Khan T M, Kido J and Kippelen B 2016 Simultaneous cross-linking and p-doping of a polymeric semiconductor film by immersion into a phosphomolybdic acid solution for use in organic solar cells *Chem. Commun.* **52** 3825–7
- [85] Kolesov V A *et al* 2017 Solution-based electrical doping of semiconducting polymer films over a limited depth *Nat. Mater.* **16** 474–81
- [86] Larraín F A, Fuentes-Hernandez C, Chou W F, Rodríguez-Toro V A, Huang T Y, Toney M F and Kippelen B 2018 Stable solvent for solution-based electrical doping of semiconducting polymer films and its application to organic solar cells *Energy Environ. Sci.* **11** 2216–24
- [87] Jia X, Shen L, Yao M, Liu Y, Yu W, Guo W and Ruan S 2015 Highly efficient low-bandgap polymer solar cells with solution-processed and annealing-free phosphomolybdic acid as hole-transport layers *ACS Appl. Mater. Interfaces* **7** 5367–72
- [88] Ji G *et al* 2018 Fully coated semitransparent organic solar cells with a doctor-blade-coated composite anode buffer layer of phosphomolybdic acid and PEDOT:PSS and a spray-coated silver nanowire top electrode *ACS Appl. Mater. Interfaces* **10** 943–54
- [89] Lu S, Lin H, Zhang S, Hou J and Choy W C H 2017 A switchable interconnecting layer for high performance tandem organic solar cell *Adv. Energy Mater.* **7** 1–10
- [90] Dong G, Xia D, Yang Y, Shenga L, Ye T and Fan R 2017 Keggin-type PMo11V as a P-type dopant for enhancing the efficiency and reproducibility of perovskite solar cells *ACS Appl. Mater. Interfaces* **9** 2378–86
- [91] Dong Y, Zhang J, Yang Y, Qiu L, Xia D, Lin K, Wang J, Fan X and Fan R 2019 Self-assembly of hybrid oxidant POM@Cu-BTC for enhanced efficiency and long-term stability of perovskite solar cells *Angew. Chem., Int. Ed.* **58** 1–7
- [92] Zhang Y, Wang Y, Sun Z, Li F, Tao R, Jin Z and Xu L 2017 Large grain growth for hole-conductor-free fully printable perovskite solar cells via polyoxometalate molecular doping *Chem. Commun.* **53** 2290–3
- [93] Lu K, Yuan J, Peng J, Huang X, Cui L, Jiang Z, Wang H-Q and Ma W 2013 New solution-processable small molecules as hole-transporting layer in efficient polymer solar cells *J. Mater. Chem. A* **1** 14253–61
- [94] Subbiah J, Amb C M, Irfan I, Gao Y, Reynolds J R and So F 2012 High-efficiency inverted polymer solar cells with double interlayer *ACS Appl. Mater. Interfaces* **4** 866–70
- [95] Hyosung C, Kim H B, Ko S J, Kim J Y and Heeger A J 2015 An organic surface modifier to produce a high work function transparent electrode for high performance polymer solar cells *Adv. Mater.* **27** 892–6
- [96] Bach U, Lupo D, Comte P, Moser J E, Weissörtel F, Salbeck J, Spreitzer H and Grätzel M 1998 Solid-state dye-sensitized mesoporous TiO_2 solar cells with high photon-to-electron conversion efficiencies *Nature* **395** 583–5
- [97] Burschka J, Dualé A, Kessler F, Baranoff E, Cevy-Ha N L, Yi C, Nazeeruddin M K and Grätzel M 2011 $\text{Tris(2-(1H-pyrazol-1-yl)pyridine)cobalt(III)}$ as p-type dopant for organic semiconductors and its application in highly efficient solid-state dye-sensitized solar cells *J. Am. Chem. Soc.* **133** 18042–5
- [98] Bi D *et al* 2016 Efficient luminescent solar cells based on tailored mixed-cation perovskites *Sci. Adv.* **2** 1–7
- [99] Luo J, Jia C, Wan Z, Han F, Zhao B and Wang R 2017 The novel dopant for hole-transporting material opens a new processing route to efficiently reduce hysteresis and improve stability of planar perovskite solar cells *J. Power Sources* **342** 886–95
- [100] Li Z, Tinkham J, Schulz P, Yang M, Kim D H, Berry J, Sellinger A and Zhu K 2017 Acid additives enhancing the conductivity of Spiro-OMeTAD toward high-efficiency

- and hysteresis-less planar perovskite solar cells *Adv. Energy Mater.* **7** 1601451
- [101] Jeon N J, Lee H G, Kim Y C, Seo J, Noh J H, Lee J and Seok I S 2014 O-methoxy substituents in spiro-OMeTAD for efficient inorganic-organic hybrid perovskite solar cells *J. Am. Chem. Soc.* **136** 7837–40
- [102] Burschka J 2013 *High Performance Solid-state Mesoscopic Solar Cells* (Switzerland: Ecole Polytechnique Fdrale de Lausanne)
- [103] Dhingra P, Singh P, Rana P J S, Garg A and Kar P 2016 Hole-transporting materials for perovskite-sensitized solar cells *Energy Technol.* **4** 891–938
- [104] Hu Z, Fu W, Yan L, Miao J, Yu H, He Y, Goto O, Meng H, Chen H and Huang W 2016 Effects of heteroatom substitution in spiro-bifluorene hole transport materials *Chem. Sci.* **7** 5007–12
- [105] Franckevičius M, Mishra A, Kreuzer F, Luo J, Zakeeruddin S M and Grätzel M 2015 A dopant-free spirobi[cyclopenta[2,1-b:3,4-b']dithiophene] based hole-transport material for efficient perovskite solar cells *Mater. Horiz.* **2** 613–8
- [106] Bi D, Xu B, Gao P, Sun L, Grätzel M and Hagfeldt A 2016 Facile synthesized organic hole transporting material for perovskite solar cell with efficiency of 19.8% *Nano Energy* **23** 138–44
- [107] Xu B, Bi D, Hua Y, Liu P, Cheng M, Grätzel M, Kloo L, Hagfeldt A and Sun L 2016 A low-cost spiro[fluorene-9,9'-xanthene]-based hole transport material for highly efficient solid-state dye-sensitized solar cells and perovskite solar cells *Energy Environ. Sci.* **9** 873–7
- [108] Zhang J *et al* 2016 Constructive effects of alkyl chains: A strategy to design simple and non-spiro hole transporting materials for high-efficiency mixed-ion perovskite solar cells *Adv. Energy Mater.* **6** 1502536
- [109] Hua Y *et al* 2016 Facile synthesis of fluorene-based hole transport materials for efficient perovskite solar cells and solid-state dye-sensitized solar cells *Nano Energy* **26** 108–13
- [110] Saliba M *et al* 2016 A molecularly engineered hole-transporting material for efficient perovskite solar cells *Nat. Energy* **1** 1–7
- [111] Xu B *et al* 2017 Tailor-making low-cost spiro[fluorene-9,9'-xanthene]-based 3D oligomers for perovskite solar cells *Chem* **2** 676–87
- [112] Rakstys K, Paek S, Sohail M, Gao P, Cho K T, Gratia P, Lee Y, Dahmen K H and Nazeeruddin M K 2016 A highly hindered bithiophene-functionalized dispiro-oxepine derivative as an efficient hole transporting material for perovskite solar cells *J. Mater. Chem. A* **4** 18259–64
- [113] Chen Y C, Huang S K, Li S S, Tsai Y Y, Chen C P, Chen C W and Chang Y J 2018 Facilely synthesized spiro[fluorene-9,9'-phenanthrene-10''-one] in donor-acceptor-donor hole-transporting materials for perovskite solar cells *ChemSusChem* **11** 3225–33
- [114] Sun Y *et al* 2018 A new hole transport material for efficient perovskite solar cells with reduced device cost *Sol. RRL* **2** 1700175
- [115] Jeon N J, Na H, Jung E H, Yang T Y, Lee Y G, Kim G, Shin H W, Seok S I, Lee J and Seo J 2018 A fluorene-terminated hole-transporting material for highly efficient and stable perovskite solar cells *Nat. Energy* **3** 682–9
- [116] Li H, Fu K, Boix P P, Wong L H, Hagfeldt A, Grätzel M, Mhaisalkar S G and Grimsdale A C 2014 Hole-transporting small molecules based on thiophene cores for high efficiency perovskite solar cells *ChemSusChem* **7** 3420–5
- [117] Zimmermann I, Urieta-Mora J, Gratia P, Aragón J, Grancini G, Molina-Ontoria A, Ortí E, Martín N and Nazeeruddin M K 2017 High-efficiency perovskite solar cells using molecularly engineered, thiophene-rich, hole-transporting materials: influence of alkyl chain length on power conversion efficiency *Adv. Energy Mater.* **7** 1601674
- [118] Zhang F *et al* 2017 Over 20% PCE perovskite solar cells with superior stability achieved by novel and low-cost hole-transporting materials *Nano Energy* **41** 469–75
- [119] García-Benito I, Zimmermann I, Urieta-Mora J, Aragón J, Molina-Ontoria A, Ortí E, Martín N and Nazeeruddin M K 2017 Isomerism effect on the photovoltaic properties of benzotrithiophene-based hole-transporting materials *J. Mater. Chem. A* **5** 8317–24
- [120] Zhao X *et al* 2016 A novel one-step synthesized and dopant-free hole transport material for efficient and stable perovskite solar cells *J. Mater. Chem. A* **4** 16330–4
- [121] Zhang F, Liu X, Yi C, Bi D, Luo J, Wang S, Li X, Xiao Y, Zakeeruddin S M and Grätzel M 2016 Dopant-free donor (D)– π –D– π –D conjugated hole-transport materials for efficient and stable perovskite solar cells *ChemSusChem* **9** 2578–85
- [122] Zhang F *et al* 2016 A novel dopant-free triphenylamine based molecular “butterfly” hole-transport material for highly efficient and stable perovskite solar cells *Adv. Energy Mater.* **6** 1600401
- [123] Park S, Heo J H, Yun J H, Jung T S, Kwak K, Ko M J, Cheon C H, Kim J Y, Im S H and Son H J 2016 Effect of multi-armed triphenylamine-based hole transporting materials for high performance perovskite solar cells *Chem. Sci.* **7** 5517–22
- [124] Nishimura H, Ishida N, Shimazaki A, Wakamiya A, Saeki A, Scott L T and Murata Y 2015 Hole-transporting materials with a two-dimensionally expanded π -system around an azulene core for efficient perovskite solar cells *J. Am. Chem. Soc.* **137** 15656–9
- [125] Park S, Heo J H, Cheon C H, Kim H, Im S H and Son H J 2015 A [2,2] paracyclophane triarylamine-based hole-transporting material for high performance perovskite solar cells *J. Mater. Chem. A* **3** 24215–20
- [126] Xu P, Liu P, Li Y, Xu B, Kloo L, Sun L and Hua Y 2018 D–A–D-typed hole transport materials for efficient perovskite solar cells: tuning photovoltaic properties via the acceptor group *ACS Appl. Mater. Interfaces* **10** 19697–703
- [127] Xue R, Zhang M, Xu G, Zhang J, Chen W, Chen H, Yang M, Cui C, Li Y and Li Y 2018 Molecular design with silicon core: toward commercially available hole transport materials for high-performance planar p-i-n perovskite solar cells *J. Mater. Chem. A* **6** 404–13
- [128] Park S J *et al* 2017 Inverted planar perovskite solar cells with dopant free hole transporting material: Lewis base-assisted passivation and reduced charge recombination *J. Mater. Chem. A* **5** 13220–7
- [129] Rakstys K *et al* 2015 Triazatruxene-based hole transporting materials for highly efficient perovskite solar cells *J. Am. Chem. Soc.* **137** 16172–8
- [130] Sung S D, Kang M S, Choi I T, Kim H M, Kim H, Hong M, Kim H K and Lee W I 2014 14.8% Perovskite solar cells employing carbazole derivatives as hole transporting materials *Chem. Commun.* **50** 14161–3
- [131] Kang M S, Sung S D, Choi I T, Kim H, Hong M, Kim J, Lee W I and Kim H K 2015 Novel carbazole-based hole-transporting materials with star-shaped chemical structures for perovskite-sensitized solar cells *ACS Appl. Mater. Interfaces* **7** 22213–7
- [132] Gratia P, Magomedov A, Malinauskas T, Daskeviciene M, Abate A, Ahmad S, Grätzel M, Getautis V and Nazeeruddin M K 2015 A methoxydiphenylamine-substituted carbazole twin derivative: an efficient

- hole-transporting material for perovskite solar cells *Angew. Chem., Int. Ed.* **54** 11409–13
- [133] Magomedov A *et al* 2018 Diphenylamine-substituted carbazole-based hole transporting materials for perovskite solar cells: influence of isomeric derivatives *Adv. Funct. Mater.* **28** 1–13
- [134] Yin C *et al* 2018 Low-cost N,N''-bicarbazole-based dopant-free hole-transporting materials for large-area perovskite solar cells *Adv. Energy Mater.* **8** 1–10
- [135] Reddy S S, Gunasekar K, Heo J H, Im S H, Kim C S, Kim D H, Moon J H, Lee J Y, Song M and Jin S H 2016 Highly efficient organic hole transporting materials for perovskite and organic solar cells with long-term stability *Adv. Mater.* **28** 686–93
- [136] Daskeviciene M *et al* 2017 Carbazole-based enamine: low-cost and efficient hole transporting material for perovskite solar cells *Nano Energy* **32** 551–7
- [137] Liu Y, Hong Z, Chen Q, Chen H, Chang W H, Yang Y M, Song T-B and Yang Y 2016 Perovskite solar cells employing dopant-free organic hole transport materials with tunable energy levels *Adv. Mater.* **28** 440–6
- [138] Shi Y, Hou K, Wang Y, Wang K, Ren H C, Pang M Y, Chen F and Zhang S 2016 Two methoxyaniline-substituted dibenzofuran derivatives as hole-transport materials for perovskite solar cells *J. Mater. Chem. A* **4** 5415–22
- [139] Yang L, Cai F, Yan Y, Li J, Liu D, Pearson A J and Wang T 2017 Conjugated small molecule for efficient hole transport in high-performance p-i-n type perovskite solar cells *Adv. Funct. Mater.* **27** 1702613
- [140] Zhang H, Wu Y, Zhang W, Li E, Shen C, Jiang H, Tian H and Zhu W H 2018 Low cost and stable quinoxaline-based hole-transporting materials with a D–A–D molecular configuration for efficient perovskite solar cells *Chem. Sci.* **9** 5919–28
- [141] Wu F, Ji Y, Wang R, Shan Y and Zhu L 2017 Molecular engineering to enhance perovskite solar cell performance: incorporation of benzothiadiazole as core unit for low cost hole transport materials *Dyes Pigm.* **143** 356–60
- [142] Wu F, Ji Y, Zhong C, Liu Y, Tan L and Zhu L 2017 Fluorine-substituted benzothiadiazole-based hole transport materials for highly efficient planar perovskite solar cells with a FF exceeding 80% *Chem. Commun.* **53** 8719–22
- [143] Pham H D, Do T T, Kim J, Charbonneau C, Manzhos S, Feron K, Tsoi W C, Durrant J R, Jain S M and Sonar P 2018 Molecular engineering using an anthanthrone dye for low-cost hole transport materials: a strategy for dopant-free, high-efficiency, and stable perovskite solar cells *Adv. Energy Mater.* **8** 1703007
- [144] Wu F, Shan Y, Qiao J, Zhong C, Wang R, Song Q and Zhu L 2017 Replacement of biphenyl by bipyridine enabling powerful hole transport materials for efficient perovskite solar cells *ChemSusChem* **10** 3833–8
- [145] Li Y *et al* 2016 Highly efficient p-i-n perovskite solar cells utilizing novel low-temperature solution-processed hole transport materials with linear π -conjugated structure *Small* **12** 4902–8
- [146] Yusoff A R B M, Kim J, Jang J and Nazeeruddin M K 2016 New horizons for perovskite solar cells employing DNA-CTMA as the hole-transporting material *ChemSusChem* **9** 1736–42
- [147] Kesters J, Verstappen P, Kelchtermans M, Lutsen L, Vanderzande D and Maes W 2015 Porphyrin-based bulk heterojunction organic photovoltaics: the rise of the colors of life *Adv. Energy Mater.* **5** 1500218
- [148] Ladomenou K, Kitsopoulos T N, Sharma G D and Coutsolelos A G 2014 The importance of various anchoring groups attached on porphyrins as potential dyes for DSSC applications *RSC Adv.* **4** 21379–404
- [149] Ladomenou K, Nikolaou V, Charalambidis G and Coutsolelos A G 2016 Artificial hemes for DSSC and/or BHI applications *Dalton Trans.* **45** 1111–26
- [150] Nikolaou V, Charisiadis A, Charalambidis G, Coutsolelos A G and Odobel F 2017 Recent advances and insights in dye-sensitized NiO photocathodes for photovoltaic devices *J. Mater. Chem. A* **5** 21077–113
- [151] Panda M K, Ladomenou K and Coutsolelos A G 2012 Porphyrins in bio-inspired transformations: light-harvesting to solar cell *Coord. Chem. Rev.* **256** 2601–27
- [152] Mathew S, Yella A, Gao P, Humphry-Baker R, Curchod B F E, Ashari-Astani N, Tavernelli I, Rothlisberger U, Nazeeruddin M K and Grätzel M 2014 Dye-sensitized solar cells with 13% efficiency achieved through the molecular engineering of porphyrin sensitizers *Nat. Chem.* **6** 242–7
- [153] Umeyama T, Takamatsu T, Tezuka N, Matano Y, Araki Y, Wada T, Yoshikawa O, Sagawa T, Yoshikawa S and Imahori H 2009 Synthesis and photophysical and photovoltaic properties of porphyrin–furan and –thiophene alternating copolymers *J. Phys. Chem. C* **113** 10798–806
- [154] Mahmood A, Hu J Y, Xiao B, Tang A, Wang X and Zhou E 2018 Recent progress in porphyrin-based materials for organic solar cells *J. Mater. Chem. A* **6** 16769–97
- [155] Sharma G D, Daphnomili D, Biswas S and Coutsolelos A G 2013 New soluble porphyrin bearing a pyridinylethynyl group as donor for bulk heterojunction solar cells *Org. Electron.* **14** 1811–9
- [156] Sharma G D, Siddiqui S A, Nikiforou A, Zervaki G E, Georgakaki I, Ladomenou K and Coutsolelos A G 2015 A mono(carboxy)porphyrin-triazine-(bodipy)2 triad as a donor for bulk heterojunction organic solar cells *J. Mater. Chem. C* **3** 6209–17
- [157] Nian L, Gao K, Liu F, Kan Y, Jiang X, Liu L, Xie Z, Peng X, Russell T P and Ma Y 2016 11% efficient ternary organic solar cells with high composition tolerance via integrated near-IR sensitization and interface engineering *Adv. Mater.* **28** 8184–90
- [158] Xiao L, Gao K, Zhang Y, Chen X, Hou L, Cao Y and Peng X 2016 A complementary absorption small molecule for efficient ternary organic solar cells *J. Mater. Chem. A* **4** 5288–93
- [159] Hasani A, Gavani J N, Pashaki R M, Baseghi S, Salehi A, Heo D, Kim S Y and Mahyari M 2017 Poly(3,4 ethylenedioxythiophene): poly(styrenesulfonate)/iron(III) porphyrin supported on S and N Co-doped graphene quantum dots as a hole transport layer in polymer solar cells *Sci. Adv. Mater.* **9** 1616–25
- [160] Chou H H, Chiang Y H, Li M H, Shen P S, Wei H J, Mai C L, Chen P and Yeh C Y 2016 Zinc porphyrin-ethynylaniline conjugates as novel hole-transporting materials for perovskite solar cells with power conversion efficiency of 16.6% *ACS Energy Lett.* **1** 956–62
- [161] Chiang Y H, Chou H H, Cheng W T, Li Y R, Yeh C Y and Chen P 2018 Porphyrin dimers as hole-transporting layers for high-efficiency and stable perovskite solar cells *ACS Energy Lett.* **3** 1620–6
- [162] Chen S, Liu P, Hua Y, Li Y, Kloo L, Wang X, Ong S, Wong W and Zhu X 2017 Study of arylamine substituted porphyrins as hole transporting materials in high performance perovskite solar cells *ACS Appl. Mater. Interfaces* **9** 13231–9
- [163] Lee U H, Azmi R, Sinaga S, Hwang S, Eom S H, Kim T W, Yoon S C, Jang S Y and Jung I H 2017 Diphenyl-2-pyridylamine-substituted porphyrins as hole-transporting materials for perovskite solar cells *ChemSusChem* **10** 3780–7

- [164] Azmi R, Lee U H, Wibowo F T A, Eom S H, Yoon S C, Jang S Y and Jung I H 2018 Performance improvement in low-temperature-processed perovskite solar cells by molecular engineering of porphyrin-based hole transport materials *ACS Appl. Mater. Interfaces* **10** 35404–10
- [165] Cao J, Lv X, Zhang P, Chuong T T, Wu B, Feng X, Shan C, Liu J and Tang Y 2018 Plant sunscreen and Co(II)/(III) porphyrins for UV-resistant and thermally stable perovskite solar cells: from natural to artificial *Adv. Mater.* **30** 1–9
- [166] Yella A, Lee H-W, Tsao H N, Yi C, Chandiran A K, Nazeeruddin M K, Diau E W-G, Yeh C-Y, Zakeeruddin S M and Grätzel M 2011 Porphyrin-sensitized solar cells with cobalt (II/III)-based redox electrolyte exceed 12 percent efficiency *Science* **334** 629–34
- [167] Gao K, Zhu Z, Xu B, Jo S B, Kan Y, Peng X and Jen A K Y 2017 Highly Efficient porphyrin-based OPV/perovskite hybrid solar cells with extended photoresponse and high fill factor *Adv. Mater.* **29** 1703980
- [168] Tran V-H, Eom S H, Yoon S C, Kim S-K and Lee S-H 2019 Enhancing device performance of inverted organic solar cells with $\text{SnO}_2/\text{Cs}_2\text{CO}_3$ as dual electron transport layers *Org. Electron.* **68** 85–95
- [169] Polydorou E *et al* 2016 Surface passivation effect by fluorine plasma treatment on ZnO for efficiency and lifetime improvement of inverted polymer solar cells *J. Mater. Chem. A* **4** 11844–58
- [170] Liu D and Kelly T L 2014 Perovskite solar cells with a planar heterojunction structure prepared using room-temperature solution processing techniques *Nat. Photon.* **8** 133–8
- [171] Ke W *et al* 2015 Low-temperature solution-processed tin oxide as an alternative electron transporting layer for efficient perovskite solar cells *J. Am. Chem. Soc.* **137** 6730–3
- [172] Li S S *et al* 2015 Bulk intermixing-type perovskite $\text{CH}_3\text{NH}_3\text{PbI}_3/\text{TiO}_2$ nanorod hybrid solar cells *Nanoscale* **7** 14532–7
- [173] Wojciechowski K, Saliba M, Leijtens T, Abate A and Snaith H J 2014 Sub-150 °C processed meso-superstructured perovskite solar cells with enhanced efficiency *Energy Environ. Sci.* **7** 1142–7
- [174] Wojciechowski K, Leijtens T, Siprova S, Schlueter C, Hörantner M T, Wang J T W, Li C Z, Jen A K Y, Lee T L and Snaith H J 2015 C_{60} as an efficient n-type compact layer in perovskite solar cells *J. Phys. Chem. Lett.* **6** 2399–405
- [175] Jeng J Y, Chiang Y F, Lee M H, Peng S R, Guo T F, Chen P and Wen T C 2013 $\text{CH}_3\text{NH}_3\text{PbI}_3$ perovskite/fullerene planar-heterojunction hybrid solar cells *Adv. Mater.* **25** 3727–32
- [176] Roldán-Carmona C, Malinkiewicz O, Soriano A, Mínguez Espallargas G, García A, Reinecke P, Kroyer T, Dar M I, Nazeeruddin M K and Bolink H J 2014 Flexible high efficiency perovskite solar cells *Energy Environ. Sci.* **7** 994–7
- [177] Vasilopoulou M *et al* 2017 Hydrogen and nitrogen codoping of anatase TiO_2 for efficiency enhancement in organic solar cells *Sci. Rep.* **7** 1–11
- [178] Ma J, Lin Z, Guo X, Zhou L, Su J, Zhang C, Yang Z, Chang J, Liu S F and Hao Y 2019 Low-temperature solution-processed ZnO electron transport layer for highly efficient and stable planar perovskite solar cells with efficiency over 20% *Sol. RRL* **3** 1900096
- [179] Noh M F M, Teh C H, Daik R, Lim E L, Yap C C, Ibrahim M A, Ahmad Ludin N, Mohd Yusoff A R B, Jang J and Teridi M A M 2018 The architecture of the electron transport layer for a perovskite solar cell *J. Mater. Chem. C* **6** 682–712
- [180] Mahmood K, Sarwar S and Mehran M T 2017 Current status of electron transport layers in perovskite solar cells: materials and properties *RSC Adv.* **7** 17044–62
- [181] Agnihotri P, Sahu S and Tiwari S 2018. Recent advances & perspectives in electron transport layer of organic solar cells for efficient solar energy harvesting. *2017 Int. Conf. Energy, Commun. Data Anal. Soft Comput. ICECDS. 2017* pp 1568–73
- [182] Shekhar H, Kleven R T, Peng T, Palaniappan A, Karani K B, Huang S, McPherson D D and Holland C K 2019 In vitro characterization of sonothrombolysis and echocontrast agents to treat ischemic stroke *Sci. Rep.* **9** 1–13
- [183] Mohammadian-Sarcheshmeh H and Mazloum-Ardakani M 2018 Recent advancements in compact layer development for perovskite solar cells *Heliyon* **4** e00912
- [184] Ansari F, Nazari P, Payandeh M, Asl F M, Abdollahi-Nejand B, Ahmadi V, Taghiloo J and Salavati-Niasari M 2018 Novel nanostructured electron transport compact layer for efficient and large-area perovskite solar cells using acidic treatment of titanium layer *Nanotechnol.* **29** 075404
- [185] Jin S H, Jun G H, Hong S H and Jeon S 2012 Conformal coating of titanium suboxide on carbon nanotube networks by atomic layer deposition for inverted organic photovoltaic cells *Carbon NY* **50** 4483–8
- [186] Oo T Z, Devi Chandra R, Yantara N, Prabhakar R R, Wong L H, Mathews N and Mhaisalkar S G 2012 Zinc tin oxide (ZTO) electron transporting buffer layer in inverted organic solar cell *Org. Electron.* **13** 870–4
- [187] Liu S, Zhang K, Lu J, Zhang J, Yip H, Huang F and Cao Y 2013 High-efficiency polymer solar cells via the incorporation of an amino-functionalized conjugated metallopolymer as a cathode interlayer *J. Am. Chem. Soc.* **135** 15326–9
- [188] Hu Z, Zhang J, Liu Y, Hao Z, Zhang X and Zhao Y 2011 Influence of ZnO interlayer on the performance of inverted organic photovoltaic device *Sol. Energy Mater. Sol. Cells* **95** 2126–30
- [189] Ouyang D, Huang Z and Choy W C H 2019 Solution-processed metal oxide nanocrystals as carrier transport layers in organic and perovskite solar cells *Adv. Funct. Mater.* **29** 1804660
- [190] Vourdas N, Papadimitropoulos G, Kostis I, Vasilopoulou M and Davazoglou D 2012 Substoichiometric hot-wire WO_x films deposited in reducing environment *Thin Solid Films* **520** 3614–9
- [191] Papamakarios V *et al* 2016 Surface modification of ZnO layers via hydrogen plasma treatment for efficient inverted polymer solar cells *ACS Appl. Mater. Interfaces* **8** 1194–205
- [192] Ren C *et al* 2019 Double electron transport layers for efficient and stable organic–inorganic hybrid perovskite solar cells *Org. Electron.* **70** 292–9
- [193] Zheng S, Wang G, Liu T, Lou L, Xiao S and Yang S 2019 Materials and structures for the electron transport layer of efficient and stable perovskite solar cells *Sci. China Chem.* **62** 800–9
- [194] Sanchez J G, Balderrama V S, Estrada M, Pallares J and Marsal L F 2019. High efficient inverted polymer solar cells with solution-processed electron transport layer. *Lat. Am. Electron Devices Conf. LAEDC* **2019** 8–10
- [195] Upama M B, Elumalai N K, Mahmud M A, Wright M, Wang D, Xu C, Haque F, Chan K H and Uddin A 2017 Interfacial engineering of electron transport layer using Caesium Iodide for efficient and stable organic solar cells *Appl. Surf. Sci.* **416** 834–44
- [196] Sun X, Ji L Y, Chen W W, Guo X, Wang H H, Lei M, Wang Q and Li Y F 2017 Halide anion-fullerene π noncovalent interactions: N-doping and a halide anion migration

- mechanism in p-i-n perovskite solar cells *J. Mater. Chem. A* **5** 20720–8
- [197] Shao Y, Xiao Z, Bi C, Yuan Y and Huang J 2014 Origin and elimination of photocurrent hysteresis by fullerene passivation in $\text{CH}_3\text{NH}_3\text{PbI}_3$ planar heterojunction solar cells *Nat. Commun.* **5** 1–7
- [198] Shao Y, Yuan Y and Huang J 2016 Correlation of energy disorder and open-circuit voltage in hybrid perovskite solar cells *Nat. Energy* **1** 15001
- [199] Luo D *et al* 2018 Enhanced photovoltage for inverted planar heterojunction perovskite solar cells *Science* **360** 1442–6
- [200] Chiang C-H and Wu C-G 2016 Bulk heterojunction perovskite–PCBM solar cells with high fill factor *Nat. Photon.* **10** 196–200
- [201] Liu C, Wang K, Du P, Meng T, Yu X, Cheng S Z D and Gong X 2015 High performance planar heterojunction perovskite solar cells with fullerene derivatives as the electron transport layer *ACS Appl. Mater. Interfaces* **7** 1153–9
- [202] Cao T, Wang Z, Xia Y, Song B, Zhou Y, Chen N and Li Y 2016 Facilitating electron transportation in perovskite solar cells via water-soluble fullerenol interlayers *ACS Appl. Mater. Interfaces* **8** 18284–91
- [203] Chen Q, Wang W, Xiao S, Cheng Y, Huang F and Xiang W 2019 Improved performance of planar perovskite solar cells using an amino-terminated multifunctional fullerene derivative as the passivation layer *ACS Appl. Mater. Interfaces* **11** 27145–52
- [204] Liu H-R *et al* 2019 Pyridine-functionalized fullerene electron transport layer for efficient planar perovskite solar cells *ACS Appl. Mater. Interfaces* **11** 23982–9
- [205] Li B *et al* 2018 Anchoring fullerene onto perovskite film via grafting pyridine toward enhanced electron transport in high-efficiency solar cells *ACS Appl. Mater. Interfaces* **10** 32471–82
- [206] Liu K, Chen S, Wu J, Zhang H, Qin M, Lu X, Tu Y, Meng Q and Zhan X 2018 Fullerene derivative anchored SnO_2 for high-performance perovskite solar cells *Energy Environ. Sci.* **11** 3463–71
- [207] Cao T, Chen K, Chen Q, Zhou Y, Chen N and Li Y 2019 Fullerene derivative-modified SnO_2 electron transport layer for highly efficient perovskite solar cells with efficiency over 21% *ACS Appl. Mater. Interfaces* **11** 33825–34
- [208] Yan K, Liu Z-X, Li X, Chen J, Chen H and Li C-Z 2018 Conductive fullerene surfactants via anion doping as cathode interlayers for efficient organic and perovskite solar cells *Org. Chem. Frontiers* **5** 2845–51
- [209] Kakavelakis G, Maksudov T, Konios D, Paradisanos I, Kioseoglou G, Stratakis E and Kymakis E 2017 Efficient and highly air stable planar inverted perovskite solar cells with reduced graphene oxide doped PCBM electron transporting layer *Adv. Energy Mater.* **7** 1602120
- [210] Chang C-Y, Huang W-K, Chang Y-C, Lee K-T and Chen C-T 2016 A solution-processed n-doped fullerene cathode interfacial layer for efficient and stable large-area perovskite solar cells *J. Mater. Chem. A* **4** 640–8
- [211] Xing Y, Sun C, Yip H-L, Bazan G C, Huang F and Cao Y 2016 New fullerene design enables efficient passivation of surface traps in high performance p-i-n heterojunction perovskite solar cells *Nano Energy* **26** 7–15
- [212] Bai Y, Dong Q, Shao Y, Deng Y, Wang Q, Shen L, Wang D, Wei W and Huang J 2016 Enhancing stability and efficiency of perovskite solar cells with crosslinkable silane-functionalized and doped fullerene *Nat. Commun.* **7** 12806
- [213] Zhu Z, Chueh C, Lin F and Jen A K-Y 2016 Enhanced ambient stability of efficient perovskite solar cells by employing a modified fullerene cathode interlayer *Adv. Sci.* **3** 1600027
- [214] Khadka D B, Shirai Y, Yanagida M, Noda T and Miyano K 2018 Tailoring the open-circuit voltage deficit of wide-band-gap perovskite solar cells using alkyl chain-substituted fullerene derivatives *ACS Appl. Mater. Interfaces* **10** 22074–82
- [215] Jung J W, Jo J W and Jo W H 2011 Enhanced performance and air stability of polymer solar cells by formation of a self-assembled buffer layer from fullerene-end-capped poly(ethylene glycol) *Adv. Mater.* **23** 1782–7
- [216] O'Malley K M, Li C-Z, Yip H-L and Jen A K-Y 2012 Enhanced open-circuit voltage in high performance polymer/fullerene bulk-heterojunction solar cells by cathode modification with a C_{60} surfactant *Adv. Energy Mater.* **2** 82–6
- [217] Page Z A, Liu Y, Duzhko V V, Russell T P and Emrick T 2014 Fulleropyrrolidine interlayers: tailoring electrodes to raise organic solar cell efficiency *Science* **346** 441–4
- [218] Li S, Lei M, Lv M, Watkins S E, Tan Z, Zhu J, Hou J, Chen X and Li Y 2013 [6,6]-Phenyl-C61-butyric acid dimethylamino ester as a cathode buffer layer for high-performance polymer solar cells *Adv. Energy Mater.* **3** 1569–74
- [219] Duan C, Zhong C, Liu C, Huang F and Cao Y 2012 Highly efficient inverted polymer solar cells based on an alcohol soluble fullerene derivative interfacial modification material *Chem. Mater.* **24** 1682–9
- [220] Li C-Z, Chang C-Y, Zang Y, Ju H-X, Chueh C-C, Liang P-W, Cho N, Ginger D S and Jen A K-Y 2014 Suppressed charge recombination in inverted organic photovoltaics via enhanced charge extraction by using a conductive fullerene electron transport layer *Adv. Mater.* **26** 6262–7
- [221] Zhen J, Liu Q, Chen X, Li D, Qiao Q, Lu Y and Yang S 2016 An ethanolamine-functionalized fullerene as an efficient electron transport layer for high-efficiency inverted polymer solar cells *J. Mater. Chem. A* **4** 8072–9
- [222] Wang Y, Cong H, Yu B, Zhang Z and Zhan X 2017 Efficient inverted organic solar cells based on a fullerene derivative-modified transparent cathode *Materials* **10** 1064
- [223] Zhang B, Zhang M, Zhen J, Xie C, Liang L, Jia L, Liu Q, Chen M, Yang H and Yang S 2019 Functionalization of fullerene by polyethylene glycol toward promoted electron transport in inverted polymer solar cells *Org. Electron.* **77** 105502
- [224] Liao S-H, Jhuo H-J, Cheng Y-S and Chen S-A 2013 Fullerene derivative-doped zinc oxide nanofilm as the cathode of inverted polymer solar cells with low-bandgap polymer (PTB7-Th) for high performance *Adv. Mater.* **25** 4766–71
- [225] Liu J, Li J and Tu G 2018 Ether chain functionalized fullerene derivatives as cathode interface materials for efficient organic solar cells *Frontiers Optoelectron.* **11** 348–59
- [226] Guo J, Li Z, Wang M, Sun Y, Fu D, Liu C and Guo W 2019 Fullerene derivative layer induced phase separation and charge transport improvement for inverted polymer solar cells *Thin Solid Films* **690** 137559
- [227] Vasilopoulou M, Douvas A M, Georgiadou D G, Constantoudis V, Davazoglou D, Kennou S, Palilis L C, Daphnomili D, Coutsolelos A G and Argitis P 2014 Large work function shift of organic semiconductors inducing enhanced interfacial electron transfer in organic optoelectronics enabled by porphyrin aggregated nanostructures *Nano Res.* **7** 679–93
- [228] Vasilopoulou M *et al* 2013 Porphyrin oriented self-assembled nanostructures for efficient exciton dissociation in high-performing organic photovoltaics *J. Mater. Chem. A* **2** 182–92

- [229] Zhang K *et al* 2016 High-performance polymer tandem solar cells employing a new n-type conjugated polymer as an interconnecting layer *Adv. Mater.* **28** 4817–23
- [230] Tountas M *et al* 2018 Engineering of porphyrin molecules for use as effective cathode interfacial modifiers in organic solar cells of enhanced efficiency and stability *ACS Appl. Mater. Interfaces* **10** 20728–39
- [231] Balis N *et al* 2018 Triazine-substituted zinc porphyrin as an electron transport interfacial material for efficiency enhancement and degradation retardation in planar perovskite solar cells *ACS Appl. Energy Mater.* **1** 3216–29
- [232] Sun C *et al* 2016 Amino-functionalized conjugated polymer as an efficient electron transport layer for high-performance planar-heterojunction perovskite solar cells *Adv. Energy Mater.* **6** 1501534
- [233] Guo Q, Xu Y, Xiao B, Zhang B, Zhou E, Wang F, Bai Y, Hayat T, Alsaedi A and Tan Z 2017 Effect of energy alignment, electron mobility, and film morphology of perylene diimide based polymers as electron transport layer on the performance of perovskite solar cells *ACS Appl. Mater. Interfaces* **9** 10983–91
- [234] Heo J H, Lee S-C, Jung S-K, Kwon O-P and Im S H 2017 Efficient and thermally stable inverted perovskite solar cells by introduction of non-fullerene electron transporting materials *J. Mater. Chem. A* **5** 20615–22
- [235] Jiang K, Wu F, Yu H, Yao Y, Zhang G, Zhu L and Yan H 2018 A perylene diimide-based electron transport layer enabling efficient inverted perovskite solar cells *J. Mater. Chem. A* **6** 16868–73
- [236] Wang R, Jiang K, Yu H, Wu F, Zhu L and Yan H 2019 Efficient inverted perovskite solar cells with truxene-bridged PDI trimers as electron transporting materials *Mater. Chem. Frontiers* **3** 2137–42
- [237] Shaikh D B, Said A A, Bhosale R S, Chen W, Bhosale S V, Puyad A L, Bhosale S V and Zhang Q 2018 Dithiafulvenyl-naphthalenediimide-based small molecules as efficient non-fullerene electron-transport layer for inverted perovskite solar cells *Asian J. Org. Chem.* **7** 2294–301
- [238] Wu F, Gao W, Yu H, Zhu L, Li L and Yang C 2018 Efficient small-molecule non-fullerene electron transporting materials for high-performance inverted perovskite solar cells *J. Mater. Chem. A* **6** 4443–8
- [239] Fan B *et al* 2019 The efficient and non-hysteresis inverted non- fullerene/CH₃NH₃PbI₃ planar solar cells *Sol. Energy* **189** 307–13
- [240] Kim S S, Bae S and Jo W H 2016 A perylene diimide-based non-fullerene acceptor as an electron transporting material for inverted perovskite solar cells *RSC Adv.* **6** 19923–7
- [241] Karuppuswamy P, Chen H-C, Wang P-C, Hsu C-P, Wong K-T and Chu C-W 2018 The 3D structure of twisted benzo[ghi]perylene-triimide dimer as a non-fullerene acceptor for inverted perovskite solar cells *ChemSusChem* **11** 415–23
- [242] Miao J, Hu Z, Liu M, Umair Ali M, Goto O, Lu W, Yang T, Liang Y and Meng H 2018 A non-fullerene small molecule processed with green solvent as an electron transporting material for high efficiency p-i-n perovskite solar cells *Org. Electron.* **52** 200–5
- [243] Zhao D, Zhu Z, Kuo M-Y, Chueh -C-C and Jen A K-Y 2016 Hexaazatrinaphthylene derivatives: efficient electron-transporting materials with tunable energy levels for inverted perovskite solar cells *Angew. Chem., Int. Ed.* **55** 8999–9003
- [244] Gu P-Y, Wang N, Wu A, Wang Z, Tian M, Fu Z, Sun X W and Zhang Q 2016 An azaacene derivative as promising electron-transport layer for inverted perovskite solar cells *Chem. Asian J.* **11** 2135–8
- [245] Selzer F, Falkenberg C, Hamburger M, Baumgarten M, Müllen K, Leo K and Riede M 2014 Improved organic p-i-n type solar cells with n-doped fluorinated hexaazatrinaphthylene derivatives HATNA-F6 and HATNA-F12 as transparent electron transport material *J. Appl. Phys.* **115** 054515
- [246] Borse K, Sharma R, Gupta D and Yella A 2019 High-efficiency organic solar cells with solution processable non-fullerene acceptor as an interlayer *IEEE J. Photovolt.* **9** 1266–72
- [247] Palilis L C, Vasilopoulou M, Douvas A M, Georgiadou D G, Kennou S, Stathopoulos N A, Constantoudis V and Argitis P 2013 Solution processable tungsten polyoxometalate as highly effective cathode interlayer for improved efficiency and stability polymer solar cells *Sol. Energy Mater. Sol. Cells* **114** 205–13
- [248] Vasilopoulou M, Douvas A M, Palilis L C, Kennou S and Argitis P 2015 Old metal oxide clusters in new applications: spontaneous reduction of Keggin and Dawson polyoxometalate layers by a metallic electrode for improving efficiency in organic optoelectronics *J. Am. Chem. Soc.* **137** 6844–56
- [249] Tountas M *et al* 2017 Low work function lacunary polyoxometalates as electron transport interlayers for inverted polymer solar cells of improved efficiency and stability *ACS Appl. Mater. Interfaces* **9** 22773–87
- [250] Tountas M *et al* 2018 A silanol-functionalized polyoxometalate with excellent electron transfer mediating behavior to ZnO and TiO₂ cathode interlayers for highly efficient and extremely stable polymer solar cells *J. Mater. Chem. C* **6** 1459–69
- [251] Chen Y, Wang S, Xue L, Zhang Z, Li H, Wu L, Wang Y, Li F, Zhang F and Li Y 2016 Insights into the working mechanism of cathode interlayers in polymer solar cells via [(C₈H₁₇)₄N]₄[SiW₁₂O₄₀] *J. Mater. Chem. A* **4** 19189–96
- [252] Chen Y, Zhang S, Peng Q, Wu L, Li F and Wang Y 2017 Effect of alkyl chain length of the ammonium groups in SEPC-CIL on the performance of polymer solar cells *J. Mater. Chem. A* **5** 15294–301
- [253] Huang C, Liu C, Di Y, Li W, Liu F, Jiang L, Li J, Hao X and Huang H 2016 Efficient planar perovskite solar cells with reduced hysteresis and enhanced open circuit voltage by using PW₁₂-TiO₂ as electron transport layer *ACS Appl. Mater. Interfaces* **8** 8520–6
- [254] Dong G, Ye T, Yang Y, Sheng L, Xia D, Wang J, Fan X and Fan R 2017 SiW₁₂ -TiO₂ mesoporous layer for enhanced electron-extraction efficiency and conductivity in perovskite solar cells *ChemSusChem* **10** 2218–25
- [255] Sardashti M K, Zendeheel M, Nia N Y, Karimian D and Sheikh M 2017 High efficiency MAPbI₃ perovskite solar cell using a pure thin film of polyoxometalate as scaffold layer *ChemSusChem* **10** 3773–9
- [256] Tao R, Zhang Y, Jin Z, Sun Z and Xu L 2018 Polyoxometalate doped tin oxide as electron transport layer for low cost, hole-transport-material-free perovskite solar cells *Electrochim. Acta* **284** 10–7
- [257] Choi Y H, Kim H B, Yang I S, Sung S D, Choi Y S, Kim J and Lee W I 2017 Silicotungstate, a potential electron transporting layer for low-temperature perovskite solar cells *ACS Appl. Mater. Interfaces* **9** 25257–64
- [258] Douvas A M *et al* 2018 Multi-electron reduction of Wells–Dawson polyoxometalate films onto metallic, semiconducting and dielectric substrates *Phys. Chem. Chem. Phys.* **21** 427–37
- [259] Lee B R, Choi H, SunPark J, Lee H J, Kim S O, Kim J Y and Song M H 2011 Surface modification of metal oxide using ionic liquid molecules in hybrid organic–inorganic optoelectronic devices *J. Mater. Chem.* **21** 2051–3

- [260] Zhu F, Chen X, Zhou L, Zhou J, Yang J, Huang S and Sun Z 2014 Dependence of the performance of inverted polymer solar cells on thickness of an electron selective ZnO layer deposited by magnetron sputtering *Thin Solid Films* **551** 131–5
- [261] Yu W, Huang L, Yang D, Fu P, Zhou L, Zhang J and Li C 2015 Efficiency exceeding 10% for inverted polymer solar cells with a ZnO/ionic liquid combined cathode interfacial layer *J. Mater. Chem. A* **3** 10660–5
- [262] Fu P, Huang L, Yu W, Yang D, Liu G, Zhou L, Zhang J and Li C 2015 Efficiency improved for inverted polymer solar cells with electrostatically self-assembled BenMeIm-Cl ionic liquid layer as cathode interface layer *Nano Energy* **13** 275–82
- [263] Yu W, Zhou L, Yu S, Fu P, Guo X and Li C 2017 Ionic liquids with variable cations as cathode interlayer for conventional polymer solar cells *Org. Electron.* **42** 387–92
- [264] Yang D, Yang R, Ren X, Zhu X, Yang Z, Li C and Liu S F 2016 Hysteresis-suppressed high-efficiency flexible perovskite solar cells using solid-state ionic-liquids for effective electron transport *Adv. Mater.* **28** 5206–13
- [265] Yang D, Zhou X, Yang R, Yang Z, Yu W, Wang X, Li C, Liu S F and Chang R P H 2016 Surface optimization to eliminate hysteresis for record efficiency planar perovskite solar cells *Energy Environ. Sci.* **9** 3071–8
- [266] Wu Q, Zhou W, Liu Q, Zhou P, Chen T, Lu Y, Qiao Q and Yang S 2016 Solution-processable ionic liquid as an independent or modifying electron transport layer for high-efficiency perovskite solar cells *ACS Appl. Mater. Interfaces* **8** 34464–73
- [267] Zhang W, Ren Z, Guo Y, He X and Li X 2018 Improved the long-term air stability of ZnO-based perovskite solar cells prepared under ambient conditions via surface modification of the electron transport layer using an ionic liquid *Electrochim. Acta* **268** 539–45
- [268] Chu W, Yang J, Jiang Q, Li X and Xin J 2018 Enhancement of photovoltaic performance of flexible perovskite solar cells by means of ionic liquid interface modification in a low temperature all solution process *Appl. Surf. Sci.* **440** 1116–22
- [269] Huang C *et al* 2018 Ionic liquid modified SnO₂ nanocrystals as a robust electron transporting layer for efficient planar perovskite solar cells *J. Mater. Chem. A* **6** 22086–95
- [270] Jiang Q, Zhang L, Wang H, Yang X, Meng J, Liu H, Yin Z, Wu J, Zhang X and You J 2017 Enhanced electron extraction using SnO₂ for high-efficiency planar-structure HC(NH₂)₂PbI₃-based perovskite solar cells *Nat. Energy* **2** 16177
- [271] Sun Y, Lu S, Xu R, Liu K *et al* 2019 Collection optimization of photo-generated charge carriers for efficient organic solar cells *J. Power Sources* **412** 465–71
- [272] Xu J, Shi X, Chen J, Luan J and Yao J 2019 Optimizing solution-processed C₆₀ electron transport layer in planar perovskite solar cells by interfacial modification with solid-state ionic-liquids *J. Solid State Chem.* **276** 302–8
- [273] Li M *et al* 2018 Interface modification by ionic liquid: A promising candidate for indoor light harvesting and stability improvement of planar perovskite solar cells *Adv. Energy Mater.* **8** 1801509